Patients and methods

Patients. Participants in this study comprised 197 HCC patients who were admitted to Ehime University Hospital between 2001 and 2010. Patients taking warfarin were excluded. Serum samples were collected before treatment for HCC and were subsequently stored at −80°C. Stored serum samples were used to measure conventional DCP and NX-PVKA.

The study protocol conformed to the ethical guidelines of the 1975 Declaration of Helsinki and was approved by the institutional review board at Ehime University Hospital (approval number 1005004). This study was registered by the University hospital Medical Information Network (UMIN) Clinical Trials Registry (registration number 000007196).

Measurement of conventional DCP and NX-PVKA. Serum stored at −80°C was used for the measurement of conventional DCP and NX-PVKA. Serum levels of conventional DCP were measured by electrochemiluminescence immunoassay (ECLIA) using the Picolumi III automated analyzer with the MU-3 monoclonal antibody.[10,11] The range of detection was 5–75 000 mAU/mL. Samples above this range were diluted prior to measurement.

The method of NX-PVKA measurement was previously described in detail by Toyoda *et al.*[7] Additional experimental procedures are presented in the Supplementary Materials and Methods. The range of detection was 18–36 000 mAU/mL. Samples above this range were diluted prior to measurement.

Statistical analysis. Kaplan–Meier survival curves along with log-rank tests were used to compare survival rates of HCC patients with different NX-PVKA levels. Uni- and multivariate analyses were carried out using Cox's proportional hazards regression models, including the following predictor variables: patient sex, age, laboratory data of blood count and blood biochemistry, and tumor factors (maximum tumor size, number of tumors, and portal venous invasion). To analyze correlations between levels of tumor markers and clinical parameters, we used the log value of NX-PVKA, conventional DCP, NX-PVKA-R, and AFP. Log transformations were completed, because some serum samples indicated extremely high levels of tumor markers. Multiple linear regression analysis was performed to identify independent associations between each tumor marker and patient clinical backgrounds and tumor factors. Forward stepwise regression modeling with minimum Akaike information criterion (AIC) was used to establish a prognostic model for risk of overall survival.[12] In the analysis, we subtracted the variable with the largest P-value over 0.05, on a one-by-one basis. All statistical analyses were carried out using JMP version 9.0 software (SAS Institute, Cary, NC, USA). Statistical significance was defined as a $P < 0.05$ based on a two-tailed test.

Results

Serum levels of NX-PVKA are a significant prognostic marker for HCC patients. Baseline characteristics of patients at the time of serum collection are indicated in Table 1. Median values and ranges were 17.5 ng/mL (0.8–180 910 ng/mL) for AFP, 2.05% (0–93.2%) for AFP-L3, 75.5 mAU/mL (12–2 545 620 mAU/mL) for conventional DCP, and 47.0 mAU/mL (17–47 883 mAU/mL) for NX-PVKA. Positivity of serum levels of conventional DCP, AFP, and AFP-L3 above the thresholds of 40 mAU/mL, 20 ng/mL and 10%, were 61.2%, 46.9%, and 25.5%, respectively. Positivity of NX-PVKA-R was 40.1% with a threshold of 1.5 mAU/mL, as reported previously.[7] However, no threshold for NX-PVKA has yet been reported, and was difficult to evaluate from our cohort, since all of our subjects had HCC. Serum levels of these tumor markers, particularly those in conventional DCP, reportedly represent clinical prognostic factors among HCC patients.[13–19] We supposed that NX-PVKA and NX-PVKA-R could also be useful as prognostic markers.

Table 1 Clinical characteristics of 197 patients with hepatocellular carcinoma (HCC)

Clinical characteristics	
Male/Female (*n*)	141/56
Age (years, mean ± SD)	65.7 ± 10.5
Etiology	
HBsAg positive (*n*)	42
Anti-HCVAb positive (*n*)	120
Both positive (*n*)	1
Both negative (*n*)	34
Child-Pugh classification	
Class A (*n*)	158
Class B (*n*)	35
Class C (*n*)	4
TNM staging	
Stage I (*n*)	79
Stage II (*n*)	67
Stage III (*n*)	30
Stage IV (*n*)	21
Tumor factor	
Maximum tumor size	
≤ 30 mm (*n*)	136
> 30 mm (*n*)	61
Number of tumors	
1–3 (*n*)	161
> 3 (*n*)	36
Portal venous invasion	193 cases
VP0 (*n*)	172
VP1-4 (*n*)	21
Tumor marker	
AFP (ng/mL) median (range)	17.5 (0.8–180 910)
AFP-L3(%) median (range)	2.05 (0–93.2)
Conventional DCP (mAU/mL) median (range)	75.5 (12–2 545 620)
NX-PVKA (mAU/mL) median (range)	47 (17–47 883)
Treatment modality	
Operation (*n*)	35
TAE, PEI (*n*)	31
RFA (*n*)	92
TAE, PEI + RFA (*n*)	25
Chemotherapy (*n*)	14

AFP, alpha-fetoprotein; AFP-L3, L3 fraction of *Lens culinaris* agglutinin-reactive species of AFP; DCP, des-gamma-carboxy prothrombin; HbsAg, hepatitis B virus surface antigen; HCVAb, hepatitis C virus antibody; *n*, number of samples; PEI, percutaneous ethanol injection; RFA, radiofrequency ablation; TAE, transcatheter arterial embolization.

Table 2 Cox's proportional hazard models for overall survival according to NX-PVKA, conventional DCP, NX-PVKA-R, AFP, and AFP-L3

Tumor marker	Overall survival			
	Univarite analysis		Multivariate analysis	
	HR (95% CI)	*P* value	HR (95% CI)	*P* value
NX-PVKA (mAU/mL)	72.11 (19.14: 236.8)	< 0.0001	81.32 (15.68: 353.5)	< 0.0001
Conventional DCP (mAU/mL)	25.28 (2.571: 109.7)	0.0117	0.098 (0.004: 1.121)	0.0622
NX-PVKA-R	66.55 (6.745: 364.4)	0.0021	38.19 (2.173: 316.4)	0.0190
AFP (ng/mL)	20.28 (4.462: 64.38)	0.0007	10.11 (1.238: 54.60)	0.0334
AFP-L3 (%)	3.038 (1.134: 7.593)	0.0279	1.787 (0.563: 5.109)	0.3094

95% CI, 95% confidential interval; AFP, alpha-fetoprotein; AFP-L3, L3 fraction of *Lens culinaris* agglutinin-reactive species of AFP; DCP, des-gamma-carboxy prothrombin; HR, hazard ratio (per change in each tumor marker over entire range); NX-PVKA-R, conventional DCP divided by NX-PVKA.

The results of uni- and multivariate analyses by Cox's proportional hazard model are outlined in Table 2. Univariate analyses indicated that all tumor markers were significant predictors of overall survival. Multivariate analysis revealed NX-PVKA as the strongest independent prognostic marker for overall survival ($P < 0.0001$; hazard ratio [HR], 81.32). The HR for overall survival of NX-PVKA was larger than that of NX-PVKA-R ($P < 0.0190$; HR, 38.19). We therefore decided to examine associations between NX-PVKA and clinical features in patients with HCC.

In additional analyses, we compared overall survival between HCC patients with the following NX-PVKA levels: < 100 mAU/mL; ≥ 100 mAU/mL; < 400 mAU/mL, and finally ≥ 400 mAU/mL. Median survival in the group with < 100 mAU/mL NX-PVKA (2572 days) was significantly greater than that in the ≥ 100 mAU/mL and < 400 mAU/mL NX-PVKA groups (969 days; $P = 0.0041$) as well as in the ≥ 400 mAU/mL NX-PVKA group (392 days; $P < 0.0001$; Fig. 1a). Those analyzed data were still significant after Bonferroni correction. Survival did not differ significantly between ≥ 100 mAU/mL and < 400 mAU/mL NX-PVKA and the ≥ 400 mAU/mL NX-PVKA groups ($P = 0.0549$). In a simplified analysis, patients with a NX-PVKA level ≥ 100 mAU/mL showed significantly lower survival rates compared to patients with < 100 mAU/mL NX-PVKA (Fig. 1b; $P = 0.0001$).

We also grouped HCC patients according to Child-Pugh class A, B, or C (Fig. 1c,d). We verified the utility of NX-PVKA in predicting patient prognosis independent of hepatic functional reserve as determined by the Child-Pugh classification. Patients with a NX-PVKA level ≥ 100 mAU/mL displayed significantly lower survival rates than patients with < 100 mAU/mL NX-PVKA in both the Child-Pugh A ($P = 0.0002$) and Child-Pugh B or C subgroups ($P = 0.0026$).

To evaluate the influence of NX-PVKA levels on survival according to the TNM classification, we divided patients into two TNM subgroups: those with TNM stage I or II; and those with TNM stage III or IV (Fig. 1e,f). In both TNM subgroups, patients with higher NX-PVKA levels (≥ 100 mAU/mL) exhibited significantly lower survival rates ($P = 0.0275$ in the TNM stage I or II subgroup; $P = 0.0062$ in the TNM stage III or IV subgroup). Serum levels of NX-PVKA could thus offer a clinical prognostic factor in patients with advanced HCC.

Taken together, a ≥ 100 mAU/mL serum level of NX-PVKA could indicate poor prognosis among patients with HCC, independent of Child-Pugh or TNM classifications of cancer stage.

Tumor markers associated with clinical features and tumor factors. As illustrated in Supplemental Table S1, univariate regression analysis revealed that the following factors were significantly correlated with log NX-PVKA: bilirubin; albumin; aspartate aminotransferase; alanine aminotransferase (ALT); cholinesterase; lactate dehydrogenase, alkaline phosphatase (ALP); γ-glutamyl transpeptidase (γ-GTP); leucine aminopeptidase (LAP); C-reactive protein (CRP); total cholesterol; type IV collagen 7s; hyaluronic acid; hemoglobin; platelet count; maximum tumor size; number of tumors; and presence of portal venous invasion.

The correlation between NX-PVKA and conventional DCP was significant ($P < 0.0001$), but the correlation coefficient between conventional DCP and NX-PVKA was low ($r = 0.525$) (Fig. 2). Levels of NX-PVKA were 136 mAU/mL (19–47 883 mAU/mL) in conventional DCP-positive HCC patients, and 23 mAU/mL (17–43 mAU/mL) in conventional DCP-negative HCC patients.

Multivariate analysis was performed for each tumor marker (conventional DCP, NX-PVKA, NX-PVKA-R, AFP, and AFP-L3) using stepwise regression modeling with minimum AIC to choose the best models for each dependent variable (Supplemental Table S2). Among the factors identified in univariate analysis, sex ($P = 0.0256$), CRP ($P = 0.0105$), platelet count ($P = 0.0013$), international normalized ratio of prothrombin time (PT [international normalized ratio, INR]) ($P = 0.0065$), maximum tumor size ($P < 0.0001$), number of nodules ($P = 0.0002$), and portal venous invasion ($P = 0.0284$) were significant independent predictors of NX-PVKA. The log of NX-PVKA was significantly associated with the same factors as log conventional DCP but not log NX-PVKA-R. All tumor factors were independently associated with both log NX-PVKA and log conventional DCP. However, PT (INR) was associated with NX-PVKA ($P = 0.0065$) but not with conventional DCP ($P = 0.0545$). Furthermore, direct bilirubin was significantly associated with log NX-PVKA-R ($P = 0.0031$) but not with log NX-PVKA (not extracted).

On the other hand, ALT and type IV collagen 7S were associated with both log AFP and AFP-L3 but not with log conventional DCP or NX-PVKA (Supplemental Table S2). Both AFP and AFP-L3 were more closely related to inflammation and fibrosis due to hepatitis than NX-PVKA or conventional DCP were. All tumor factors were significantly associated with log NX-PVKA and log conventional DCP. However, only the number of tumors was associated with log AFP, while only maximum tumor size was associated with AFP-L3.

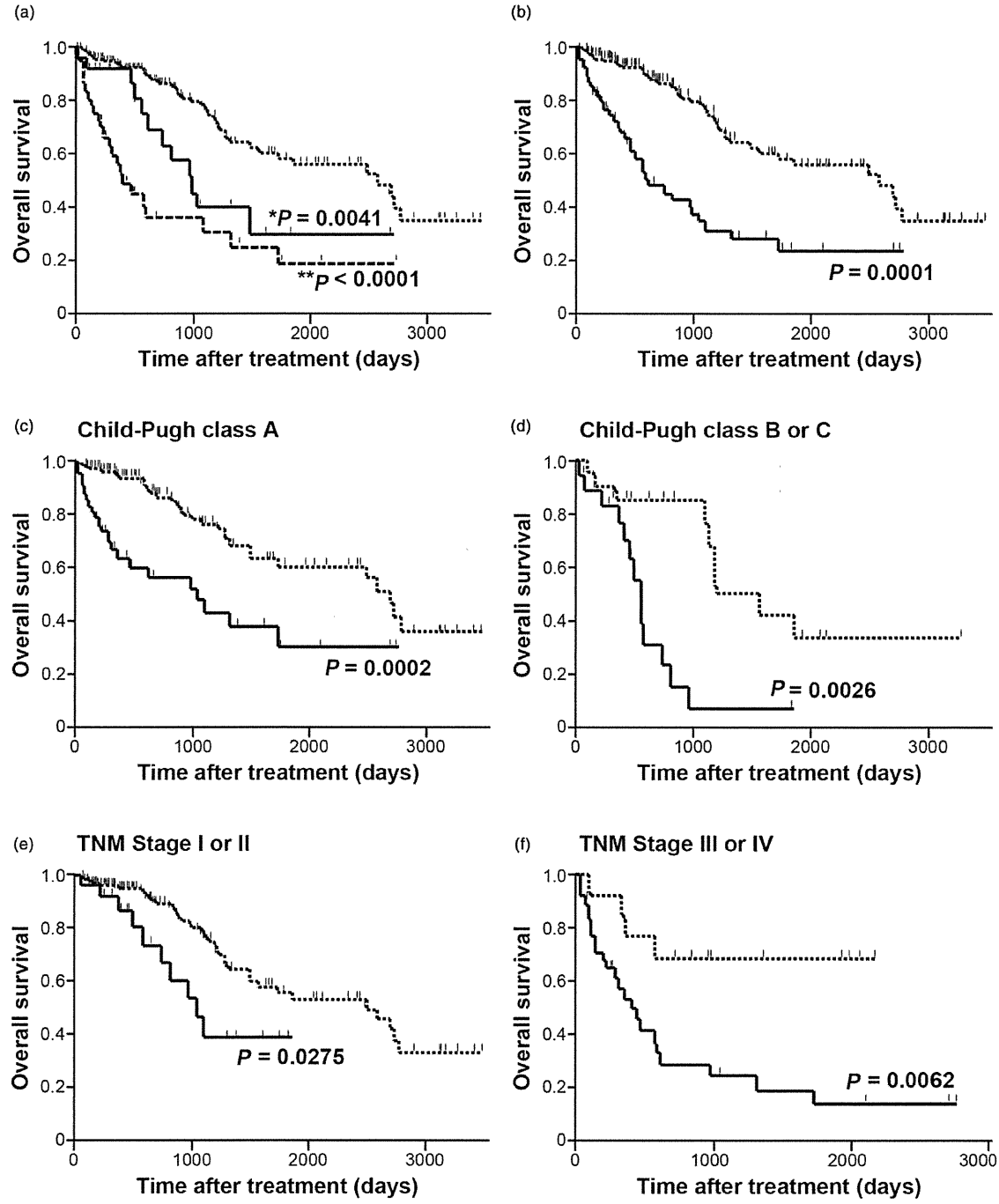

Figure 1 Overall survival of HCC patients with different levels of NX-PVKA. (a) Overall survivals of HCC patients with < 100 mAU/mL NX-PVKA, those with ≥ 100 mAU/mL and < 400 mAU/mL NX-PVKA, and those with ≥ 400 mAU/mL NX-PVKA. *Patients with 100–400 mAU/mL NX-PVKA showed significantly shorter survival than those with < 100 mAU/mL ($P = 0.0041$) and **those with ≥ 400 mAU/mL NX-PVKA ($P < 0.0001$). (b) When divided into only two groups, patients with ≥ 100 mAU/mL NX-PVKA showed significantly shorter survival than those with < 100 mAU/mL ($P = 0.0001$). This finding remained significant independent of Child-Pugh class A subgroup (c,d) and TNM stage (e,f). Kaplan-Meier survival analyses and log-rank testing were performed. Small vertical tick-marks in each figure indicate losses where patient survival was right-censored. ·····, NX-PVKA < 100; ——, 100 ≤ NX-PVKA < 400; - - - -, 400 ≤ NX-PVKA; ·····, NX-PVKA < 100; ——, NX-PVKA ≥ 100; ·····, NX-PVKA < 100; ——, NX-PVKA ≥ 100; ·····, NX-PVKA < 100; ——, NX-PVKA ≥ 100; ·····, NX-PVKA < 100; ——, NX-PVKA ≥ 100; ·····, NX-PVKA < 100; ——, NX-PVKA ≥ 100.

Table 3 Multivariate analysis by Cox's proportional hazard model for overall survival according to statistically significant prognostic factors

	HR	(95% CI)	RC	(95% CI)	*P* value
Gender [Male/Female]	3.70	(1.74: 8.86)	6.54×10^{-1}	$(2.76 \times 10^{-1}: 10.9 \times 10^{-1})$	0.0004
Albumin (g/dL)	5.11×10^{-2}	$(0.85 \times 10^{-2}: 33.9 \times 10^{-2})$	-8.04×10^{-1}	$(-12.9 \times 10^{-1}: -2.92 \times 10^{-1})$	0.0024
γ-GTP (U/L)	2.88×10	$(0.32 \times 10: 23.7 \times 10)$	4.30×10^{-3}	$(1.48 \times 10^{-3}: 7.00 \times 10^{-3})$	0.0034
LAP (U/L)	1.94×10^{-2}	$(0.05 \times 10^{-2}: 36.7 \times 10^{-2})$	-1.02×10^{-2}	$(-1.97 \times 10^{-2}: -0.26 \times 10^{-2})$	0.0071
CRP (mg/dL)	4.30×10	$(0.54 \times 10: 20.4 \times 10)$	3.17×10^{-1}	$(1.42 \times 10^{-1}: 4.48 \times 10^{-1})$	0.0017
Hyaluronic acid (ng/mL)	6.84×10	$(1.06 \times 10: 35.6 \times 10)$	1.35×10^{-3}	$(7.57 \times 10^{-4}: 1.88 \times 10^{-3})$	< 0.0001
Log NX-PVKA (mAU/mL)	1.96×10	$(0.66 \times 10: 5.65 \times 10)$	8.68×10^{-1}	$(5.52 \times 10^{-1}: 11.8 \times 10^{-1})$	< 0.0001

The risk of mortality from hepatocellular carcinoma score (ROM score) calculated by using the prognostic model results of this analysis as below. ROM score = 0.654 × (1: male, 0: female) − 0.804 × Albumin + 0.0043 × γ-GTP − 0.0102 × LAP + 0.317 × CRP + 0.00135 × Hyaluronic acid + 0.868 × Log NX-PVKA

95% CI: 95% confidential interval; CRP, C-reactive protein; DCP, des-gamma-carboxy prothrombin; HR, hazard ratio (per change in each factor over entire range); LAP, leucine aminopeptidase; PT (INR): international normalized ratio of prothrombin time; RC, risk coefficient; WB, white blood cell; γ-GTP, γ-glutamyl transpeptidase.

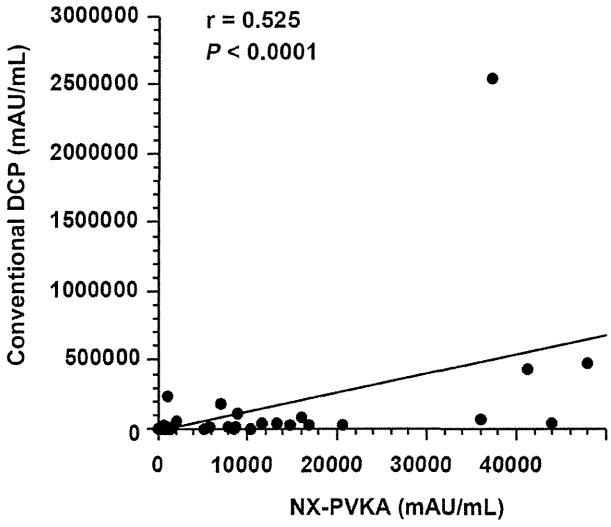

Figure 2 Correlation between NX-PVKA and conventional DCP. The correlation between NX-PVKA and conventional DCP is significant ($P < 0.0001$), although the correlation coefficient between conventional DCP and NX-PVKA is low (r = 0.525).

Results of uni- and multivariate analyses for overall survival by Cox's proportional hazard model are presented in Supplemental Table S3. Briefly, many clinical factors showed significant univariate associations with overall survival. For instance, all tumor markers, including log NX-PVKA, were significantly associated with overall survival. In addition, all three tumor factors listed in Supplemental Table S3 were significantly associated with overall survival. We excluded tumor factors from multivariate analysis and analyzed only the clinical factors listed in Supplemental Table S3. According to this analysis, log NX-PVKA was the only tumor factor that independently predicted overall survival ($P < 0.0001$). Other independent predictors of overall survival included sex ($P = 0.0001$), LAP ($P = 0.0072$), CRP ($P = 0.0094$), and hyaluronic acid ($P < 0.0001$).

Next, we sought to establish a prognostic model to estimate overall survival of patients using serum levels of log NX-PVKA. For this purpose, we used a stepwise regression model with the minimum AIC. The values identified in analyses are indicated in Table 3. The log of NX-PVKA, sex, albumin, γ-GTP, LAP, CRP, and hyaluronic acid were significant independent predictors of overall survival. From these results, we established a prognostic model for predicting overall survival in patients with HCC, which we named as the risk of mortality from HCC (ROM) score.

ROM score was calculated as follows: 0.654 × (1: male, 0: female) − 0.804 × Albumin + 0.0043 × γ-GTP − 0.0102 × LAP + 0.317 × CRP + 0.00135 × hyaluronic acid + 0.868 × log NX-PVKA

A higher ROM score indicates a lower duration of overall survival. Harrell's c-index is defined as the proportion of all usable patient pairs in which the predictions and outcome are concordant.[20] The index of correlation between ROM score and actual overall survival was 0.816.

We performed additional analyses to reveal the correlation between ROM score and overall survival of enrolled patients with HCC (Fig. 3), revealing a significant correlation (r = 0.644, $P < 0.0001$). Based on the results (Fig. 3), survival from the initiation of HCC treatment could be estimated using the following formula:

$$\log(\text{survival [days]}) = 6.311 - 0.529 \times \text{ROM score}.$$

Discussion

The present study identified serum levels of NX-PVKA, as the new variants of DCP, as the most significant prognostic tumor marker for HCC. Using NX-PVKA, we established a prognostic model that can estimate the duration of overall survival of HCC patients using clinical data.

NX-PVKA could be considered to overlap with DCP, which is produced by vitamin K deficiency.[7] With the exception of patients taking warfarin, NX-PVKA was the most effective prognostic marker among HCC patients. The clinical features associated with NX-PVKA were similar to those associated with conventional DCP but differed from those associated with AFP and AFP-L3 (Table 3). Both NX-PVKA and conventional DCP were closely related to tumor factors and platelet count, whereas AFP and AFP-L3 were not. AFP-L3 was found to be a useful

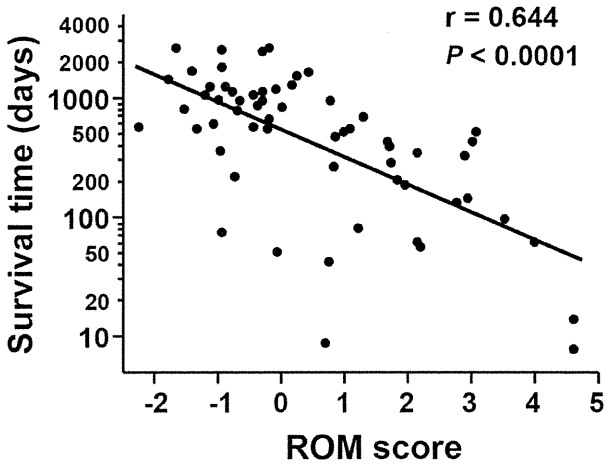

Figure 3 Correlation between risk of mortality (ROM) score from hepatocellular carcinoma (HCC) and patient. ROM score was calculated according to the following formula:
ROM score = 0.654 × (1: male, 0: female) − 0.804 × albumin + 0.0043 × γ-GTP − 0.0102 × LAP + 0.317 × CRP + 0.00135 × hyaluronic acid + 0.868 × log NX-PVKA.
ROM score correlated significantly with patient survival (r = 0.644, $P < 0.0001$). From this analysis, survival of each patient was estimated using the following equation:
log (survival [days]) = 6.311 − 0.529 × ROM score.

prognostic marker when serum concentrations of AFP were very low.[21,22] However, other reports suggest that DCP was superior to AFP in predicting disease prognosis.[23,24] Our data show general agreement with these previous reports. In addition, only NX-PVKA was associated with PT (INR). Based on univariate analysis, higher direct bilirubin correlated with high serum levels of NX-PVKA but not conventional DCP. NX-PVKA was more closely associated with hepatic functional reserve than conventional DCP was.

The expression of DCP occurs in HCC tissue, as well as in the surrounding non-HCC tissue. Inagaki *et al.* reported that the expression of DCP in both HCC and non-HCC tissues, and serum levels of DCP, were significantly related to postoperative survival in patients with HCC and liver cirrhosis.[19] Expression of DCP variants with less than 6 Glu residues was relatively higher among patients with nonmalignant liver diseases such as chronic hepatitis and liver cirrhosis than among those with HCC.[25] Hence, NX-PVKA, which comprises DCP with around 5 Glu residues, might be produced by chronically damaged liver tissue surrounding the HCC. Since HCC patients usually suffer from chronic liver injury, these notions may explain why NX-PVKA levels reflect hepatic functional reserve and best predict disease prognosis among HCC patients.

The structure of DCP contains two kringle domains similar to those of hepatocyte growth factor (HGF).[26] Moreover, DCP is thought to induce proliferation of HCC cells through HGF-like functions.[27] One reason why NX-PVKA and conventional DCP could be associated with tumor factors could be explained by the functional similarity to HGF. Direct effects of NX-PVKA on HCC tumor factors should be examined in future studies.

Multivariate analyses revealed that platelet count was positively associated with levels of both conventional DCP and NX-PVKA (Table 3). Poor hepatic functional reserve is well known to be related to decreased platelet counts in chronic liver injury.[28,29] From this perspective, the positive correlations between platelet count and both NX-PVKA and conventional DCP cannot be explained by the status of hepatic functional reserve. Others have reported that platelet count correlates with serum vascular endothelial growth factor levels in cancer patients, including those with HCC.[30] Moreover, platelet count is reportedly elevated in HCC patients with portal venous invasion[14] or extrahepatic metastasis.[18] Higher serum levels of NX-PVKA and conventional DCP with a higher platelet count would reflect tumor growth and portal venous invasion, which would contribute to the prognosis of HCC patients.

Several prognostic scoring systems have been proposed for HCC patients, including the CLIP score,[31] BCLC score,[32] and Tokyo score.[33] However, these scoring systems included tumor factors that had to be evaluated by diagnostic imaging. The present study proposed a prognostic model using only patient demographics and laboratory data. The proposed prognostic model could be useful for clinicians who do not regularly perform diagnostic imaging, or in outpatient clinics, when clinicians need to estimate approximate durations of overall survival for HCC patients. Moreover, the HCC stage could also be classified using these indices.

Several limitations must be considered when interpreting the present findings. First, this was a retrospective study of patients from a single center in Japan. Validation of the prognostic model in a prospective study is required. Second, HCC patients enrolled in this study had several etiologies of liver damage and received different treatments. Although the value of NX-PVKA was not influenced by the etiology of liver damage or treatment type, we need to perform similar experiments with a greater number of patients in each subgroup.

In conclusion, serum levels of NX-PVKA offered the most significant tumor marker predictor of prognosis among HCC patients in this study. The proposed prognostic model could be useful in estimating overall survival for HCC patients. We expect to conduct a prospective study of these findings in the near future.

Acknowledgments

The authors are grateful to Drs Jun Nishimura and Masao Uehara (EIDIA, Tokyo Japan) for their support in measuring NX-PVKA, and to Ms Satomi Nakayama, Ms Takana Fujino, and Ms Sakiko Inoh for their valuable technical assistance. This work was supported in part by a Grant-in-Aid for Scientific Research (JSPS KAKENHI 24590980 to Y.H.) and the Program for Enhancing Systematic Education in Graduate School (to S.T.) from the Japanese Ministry of Education, Culture, Sports, Science and Technology, as well as a Grant-in-Aid for Scientific Research and Development from the Japanese Ministry of Health, Labor and Welfare to Y.H.

References

1 El-Serag HM, Lenhard RK. Hepatocellular carcinoma: epidemiology and molecular carcinogenesis. *Gastroenterology* 2007; **132**: 2557–76.

2 Blanchard RA, Furie BC, Kruger SF, Waneck G, Jorgensen MJ, Furie B. Immunoassays of human prothrombin species which correlate with functional coagulation activities. *J. Lab. Clin. Med.* 1983; **101**: 242–55.
3 Liebman HA, Furie BC, Tong MJ *et al.* Des-gamma-carboxy (abnormal) prothrombin as a serum marker of primary hepatocellular carcinoma. *N. Engl. J. Med.* 1984; **310**: 1427–31.
4 Okuda H, Nakanishi T, Takatsu K *et al.* Measurement of serum levels of des-gamma-carboxy prothrombin in patients with hepatocellular carcinoma by a revised enzyme immunoassay kit with increased sensitivity. *Cancer* 1999; **85**: 812–18.
5 Bajaj SP, Price PA, Russell WA. Decarboxylation of gamma-carboxyglutamic acid residues in human prothrombin. *J. Biol. Chem.* 1982; **257**: 3726–31.
6 Naraki T, Kohno N, Saito H *et al.* γ-Carboxyglutamic acid content of hepatocellular carcinoma-associated des-γ-carboxy prothrombin. *Biochim. Biophys. Acta* 2002; **1586**: 287–98.
7 Toyoda H, Kumda T, Osaki Y *et al.* Novel method to measure serum levels of des-gamma-carboxy prothrombin for hepatocellular carcinoma in patients taking warfarin: a preliminary report. *Cancer Sci.* 2012; **103**: 921–5.
8 Aoyagi Y, Isemura M, Suzuki Y *et al.* Fucosylated alpha-fetoprotein as marker of early hepatocellular carcinoma. *Lancet* 1985; **326**: 1353–4.
9 Sato Y, Nakata K, Kato Y *et al.* Early recognition of hepatocellular carcinoma based on altered profiles of alpha-fetoprotein. *N. Engl. J. Med.* 1993; **328**: 1802–6.
10 Motohara K, Endo F, Matsuda I. Effect of vitamin K administration on acarboxyprothrombin (PIVKA-II) levels in newborns. *Lancet* 1985; **326**: 242–4.
11 Motohara K, Kuroki Y, Kan HK *et al.* Detection of vitamin deficiency by use of an enzyme-linked immunosorbent assay for circulating for circulating abnormal prothrombin. *Pediatr. Res.* 1985; **19**: 354–7.
12 Akaike H. A new look at statistical model identification. *IEEE Trans. Automat. Control* 1974; **19**: 716–23.
13 Suehiro T, Sugimachi K, Matsumata T, Itasaka H, Taketomi A, Maeda T. Protein induced by vitamin K absence or antagonist II as a prognostic marker in hepatocellular carcinoma. *Cancer* 1994; **73**: 2464–9.
14 Hagiwara S, Kudo M, Kawasaki T *et al.* Prognostic factors for portal venous invasion in patients with hepatocellular carcinoma. *J. Gastroenterol.* 2006; **41**: 1214–9.
15 Hakamada K, Kimura N, Miura T *et al.* Des-gamma-carboxy prothrombin as an important prognostic indicator in patients with small hepatocellular carcinoma. *World J. Gastroenterol.* 2008; **14**: 1370–7.
16 Kobayashi M, Ikeda K, Kawamura Y *et al.* High serum des-gamma-carboxy prothrombin level predicts poor prognosis after radiofrequency ablation of hepatocellular carcinoma. *Cancer* 2009; **115**: 571–80.
17 Yamashita Y, Tsuijita E, Takeishi K *et al.* Predictors for microinvasion of small hepatocellular carcinoma < 2 cm. *Ann. Surg. Oncol.* 2012; **19**: 2027–34.
18 Bae HM, Lee JH, Yoon JH, Kim YJ, Heo DS, Lee HS. Protein induced by vitamin K absence or antagonist-II production is a strong predictive marker for extrahepatic metastases in early hepatocellular carcinoma: a prospective evaluation. *BMC Cancer* 2011; **11**: 435–45.
19 Inagaki Y, Xu HL, Hasegawa K *et al.* Des-gamma-carboxyprothrombin in patients with hepatocellular carcinoma and liver cirrhosis. *J. Dig. Dis.* 2011; **12**: 481–8.
20 Harrell FE Jr, Lee KL, Califf RM *et al.* Regression modeling strategies for improved prognostic prediction. *Stat. Med.* 1984; **3**: 143–52.
21 Kobayashi M, Kuroiwa T, Suda T *et al.* Fucosylated fraction of alpha-fetoprotein, L3, as a useful prognostic factor in patients with hepatocellular carcinoma with special reference to low concentrations of serum alpha-fetoprotein. *Hepatol. Res.* 2007; **37**: 914–22.
22 Nouso K, Kobayashi Y, Nakamura S *et al.* Prognostic importance of fucosylated alpha-fetoprotein in hepatocellular carcinoma patients with low alpha-fetoprotein. *J. Gastroenterol. Hepatol.* 2011; **26**: 1195–200.
23 Inagaki Y, Tang W, Makuuchi M, Hasegawa K, Sugawara Y, Kokudo N. Clinical and molecular instates into the hepatocellular carcinoma tumour marker des-γ-carboxy prothrombin. *Liver Int.* 2011; **31**: 22–35.
24 Tang W, Miki K, Kokudo N *et al.* Des-gamma-carboxy prothrombin in cancer and non-cancer liver tissue of patients with hepatocellular carcinoma. *Int. J. Oncol.* 2003; **22**: 969–75.
25 Uehara S, Gotoh K, Handa H *et al.* Distribution of the heterogeneity of des-γ-carboxyprothrombin in patients with hepatocellular carcinoma. *J. Gastroenterol. Hepatol.* 2005; **20**: 1545–52.
26 Nakamura T, Nishizawa T, Hagiya M *et al.* Molecular cloning and expression of human hepatocyte growth factor. *Nature* 1989; **342**: 440–3.
27 Suzuki M, Shiraha H, Fujikawa T *et al.* Des-gamma-carboxy prothrombin is a potential autologous growth factor for hepatocellular carcinoma. *J. Biol. Chem.* 2005; **280**: 6409–15.
28 Pohl A, Behling C, Oliver D *et al.* Serum aminotransferase levels and platelet counts as predictors of degree of fibrosis in chronic hepatitis C virus infection. *Am. J. Gastroenterol.* 2001; **96**: 3142–6.
29 Shah AG, Lydecker A, Murray K *et al.* Comparison of noninvasive markers of fibrosis in patients with nonalcoholic fatty liver disease. *Clin. Gastroenterol. Hepatol.* 2009; **7**: 1104–12.
30 Koike Y, Shiratori Y, Sato S *et al.* Des-gamma-carboxy prothrombin as a useful predisposing factor for the development of portal venous invasion in patients with hepatocellular carcinoma. *Cancer* 2001; **91**: 561–9.
31 The Cancer of the Liver Italian Program (CLIP) Investigators. A new prognostic system for hepatocellular carcinoma: a retrospective study of 435 patients. *Hepatology* 1998; **28**: 751–5.
32 Llovet JM, Bru C, Bruix J. Prognosis of hepatocellular carcinoma: the BCLC staging classification. *Semin. Liver Dis.* 1999; **19**: 329–38.
33 Tateishi R, Yoshiba H, Shiina S *et al.* Proposal of a new prognostic model for hepatocellular carcinoma: an analysis of 403 patients. *Gut* 2005; **54**: 419–25.

Supporting information

Additional Supporting Information may be found in the online version of this article at the publisher's web-site:

Table S1 Univariate associations between various clinical and tumor factors and Log NX-PVKA, Log conventional DCP, Log NX-PVKA-R, Log AFP and AFP-L3.

Table S2 Multivariate stepwise regression analysis between various clinical and tumor factors and Log NX-PVKA, Log conventional DCP, Log NX-PVKA-R, Log AFP and AFP-L3.

Table S3 Cox's proportional hazard model for overall survival according to clinical and tumor factors.

Appendix S1 The method of NX-PVKA measurement.

Pathology International

Pathology International 2013; **63**: 305–310 doi:10.1111/pin.12064

Original Article

Quantification of collagen and elastic fibers using whole-slide images of liver biopsy specimens

Tokiya Abe,[1] Akinori Hashiguchi,[1] Ken Yamazaki,[1] Hirotoshi Ebinuma,[2,3] Hidetsugu Saito,[2,3] Hiromitsu Kumada,[4] Namiki Izumi,[5] Naohiko Masaki[6] and Michiie Sakamoto[1]

Departments of [1]Pathology and [2]Internal Medicine, School of Medicine, and [3]Faculty of Pharmacy, Keio University, [4]Department of Gastroenterology, Toranomon Hospital, [5]Department of Gastroenterology and Hepatology, Musashino Red Cross Hospital, Tokyo and [6]The Research Center for Hepatitis and Immunology, National Center for Global Health and Medicine, Chiba, Japan

Histological evaluation of fibrosis after a liver biopsy is crucial for evaluating the pathology of patients with chronic liver disease. Previous studies have reported quantitative analyses of fibrosis using images of collagen-stained sections. However, analysis of these studies requires manual selection of the region of interest. In addition, the quantification of elastic fibers is not considered. The present study was conducted in order to measure both the collagen and elastic fiber area ratios using Elastica van Gieson-stained whole-slide images (WSIs) of liver biopsy specimens. High-resolution WSIs provide precise color classification, enabling accurate detection of even fine collagen and elastic fibers. To minimize the influence of pre-existing fibrous tissue, median area ratios of the collagen and elastic fibers were independently calculated from the image tiles of the WSIs. These median area ratios were highly concordant with area ratios after the pre-existing fibrous tissues were manually trimmed from the WSI. Further, these median area ratios were correlated with liver stiffness as measured by transient elastography (collagen: $r = 0.73$ [$P < 0.01$], elastic: $r = 0.53$ [$P < 0.01$]). Our approach to quantifying liver fibrosis will serve as an effective tool to evaluate liver diseases in routine practice.

Key words: collagen, computer-assisted image analysis, elastin, elastography, liver fibrosis, whole-slide image

Evaluation of liver fibrosis in patients with chronic liver disease is crucial for understanding the disease state, predicting prognosis and selecting the appropriate treatment.[1,2] Although the efficacy of biochemical methods[3–6] and transient elastography for measuring liver stiffness[7] has been demonstrated, histopathological evaluation of liver biopsy specimens remains the gold standard. At present, histopathological evaluation of fibrosis using liver biopsy specimens is performed by a pathologist who stages specimens by identifying the location, degree and pattern of fibrosis, presence of architectural distortion, and regenerative nodule formation. This staging is completely dependent on the experience of the observer, and there is intra- as well as inter-individual variation in this respect.[1] To overcome these issues, quantification by imaging analysis has been suggested for evaluating the degree of liver fibrosis.[8–17] In these studies, collagen fibers were extracted from the histological image of the liver biopsy specimen, and the area occupied by the fibers relative to the area of the entire tissue specimen was quantified as a ratio. However, most of the proposed quantification methods still need an observer to define the region of interest or trim pre-existing fibrous tissue such as skin, muscle, or a large blood vessel.[8–14] An increase in collagen deposition is involved in the progression of liver fibrosis. Deposition of elastic fibers is also reportedly increased, particularly in late stages of the disease.[18–21] Thus, evaluation of elastic as well as collagen fiber deposition is crucial for the accurate evaluation of fibrosis progression; however, to our knowledge, no method that simultaneously quantifies both fibers has been reported to date.

The whole-slide imaging system, which is popular in telepathology and education, enables an entire tissue section to be digitized at a high resolution within minutes and saved as a whole-slide image (WSI).[22–24] Once the WSI is stored as digital data, it is easy to obtain individual pixel color values, and WSIs can be used for several applications including morphometrical analysis.[25–28] The purpose of this study is to develop an effective method to quantify liver fibrosis using

Correspondence: Michiie Sakamoto, MD, PhD, Department of Pathology, School of Medicine, Keio University, 35 Shinanomachi, Shinjuku-ku, Tokyo 160-8582, Japan. Email: msakamot@z5.keio.jp

Received 24 January 2013. Accepted for publication 2 May 2013.

the WSIs of liver biopsy specimens. We established a method that simultaneously quantifies the collagen and elastic fiber area ratios in Elastica van Gieson (EVG)-stained liver biopsy tissue specimens. Further, the area ratios were compared with liver stiffness as measured by transient elastography. This method of quantifying liver fibrosis using WSIs may become important in the future as a technique for assisting with pathological diagnosis.

METHODS

Samples

Liver biopsy specimens were collected from 38 chronic viral hepatitis patients (37 with chronic hepatitis C virus, and one with chronic hepatitis B virus) from four medical facilities. After obtaining the informed consent, we measured the liver stiffness by using FibroScan (Echo-Sens, Paris, France). The stiffness of the right lobe of the liver was measured by placing a probe tip into the intercostal space at a depth of 2.5–6 cm from the skin surface. Liver stiffness was measured 10 times, and the median value of these 10 measurements was used for each patient.

EVG staining

The liver biopsy specimens were formalin-fixed and paraffin-embedded. The specimens were then sliced to a thickness of 3 μm and stained with EVG. A WSI of each specimen was acquired using the NanoZoomer 2.0HT (Hamamatsu Photonics K.K., Hamamatsu, Japan) at a × 20 objective lens equivalent to 0.46 μm/pixel.

Quantification of fibrosis using WSI analysis

The WSI pixels were classified into five classes corresponding to four tissue components: collagen fibers, elastic fibers, nucleus, cytoplasm, and one non-tissue component (i.e. glass slide). The training data points, which were extracted from the portal and periportal areas in the WSI, were sampled for at least 30 points for each class. The color distributions of the five classes were analyzed in RGB color space, wherein the color analyses were done for all specimens. Subsequently, a quadratic discriminant function based on the color distribution[29] was applied in order to label each WSI pixel appropriately.

The area ratio of each tissue component is the sum of pixels for each tissue component divided by the total number of pixels of the four tissue components. The median area ratios of collagen and elastic fibers were also calculated. An image-processing program was developed using MATLAB (The MathWorks, Inc., Natick, MA, USA) for image analysis.

Statistical analysis

Relationships between measurement values were analyzed using the Spearman's rank correlation coefficient test. All *P*-values were two-tailed, and values less than 0.05 were considered statistically significant. Analyses were carried out using SPSS software (version 19.0; SPSS Inc., Chicago, IL, USA).

RESULTS

The evaluated liver biopsy specimens had an average length of 16.3 mm (SD = 3.2 mm) and an average width of 1.0 mm (SD = 0.3 mm). This is equivalent to an average of 77 mega-pixels (SD = 36 mega-pixels) in WSIs. The time required for analysis was approximately 6.3 min (SD = 3.3 min) per biopsy specimen.

Color classification of EVG-stained tissue specimens

The training data points for five classes were from the portal and periportal areas on the WSI of EVG-stained liver biopsy specimens (Fig. 1a). The extracted training data points were plotted in RGB color space (Fig. 1b). Five classes of the data points in all liver biopsy specimens were individually distinguishable in the three-dimensional color space. The composition of the color distribution of the five classes was different among the biopsy specimens, therefore, the quadratic discriminant function was designed based on the training data points in each liver biopsy specimen and applied to determine the color classification of the pixels. As a result, every pixel on the WSIs of all liver biopsy specimens was successfully labeled in the appropriate classes (Figs S1,S2). Figure 2 shows that even fine collagen and elastic fibers could be extracted from portal and periportal areas.

Measurements of the area ratios of tissue components on WSIs

The area ratio of each tissue component could be calculated from the labeled pixels. The average area ratios of collagen, elastic fibers, nucleus and cytoplasm in all biopsy specimens were 11.3% (SD = 5.1%), 3.8% (SD = 2.7%), 11.8% (SD = 5.0%) and 73.1% (SD = 8.7%), respectively. Representative WSIs and classification results of liver biopsy specimens with mild fibrosis and severe fibrosis are shown in

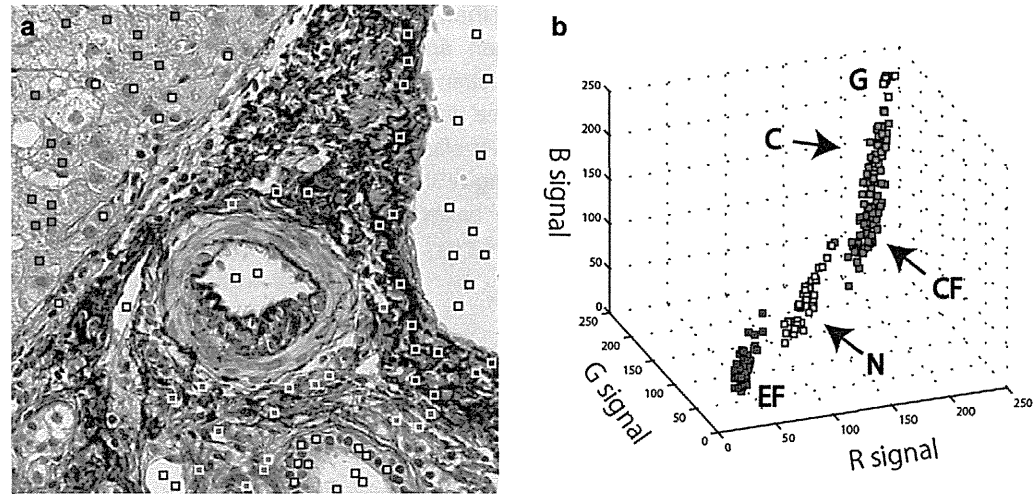

Figure 1 Sampling and color distribution. (**a**) Colored squares indicate training data points for five classes in the portal and periportal area (250 × 250 μm^2). (**b**) Color distribution of the data points in RGB color space. Each color represents a class: collagen fiber (CF), red; elastic fibers (EF), blue; cell nuclei (N), yellow; cytoplasm (C), green; glass slide (G), white.

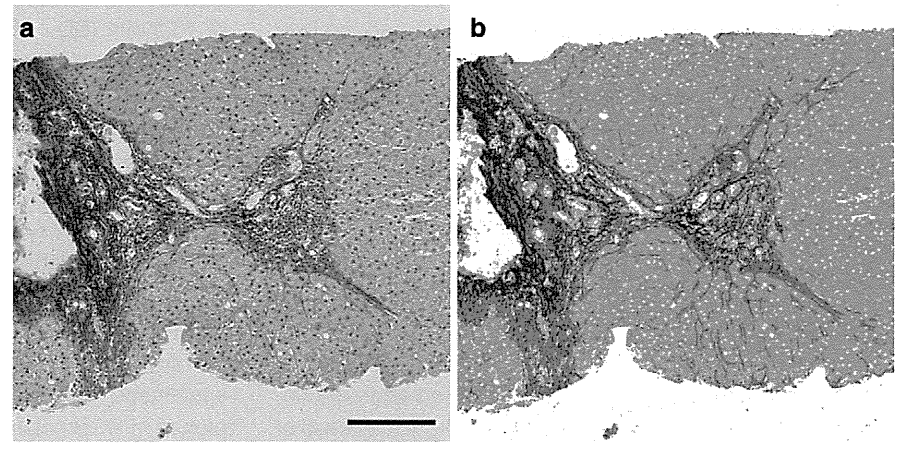

Figure 2 Color image and classification result in the portal and periportal areas (1 × 1 mm^2). In the color classification result, collagen fibers, elastic fibers, nuclei, cytoplasm, and glass slide were red, blue, yellow, green, and white, respectively. Scale bar, 0.2 mm.

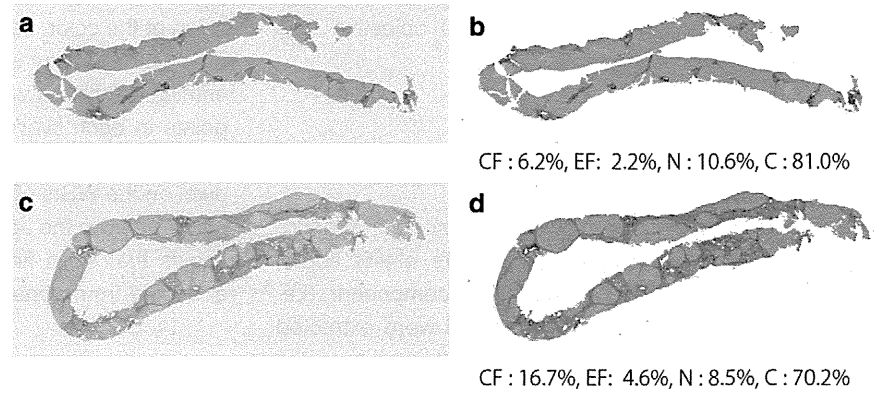

Figure 3 Measurements of area ratio on the whole-slide image. Representative whole slide images (WSIs) and classification results of liver biopsy specimen with mild fibrosis (**a,b**) and with severe fibrosis (**c,d**). The percentage indicates area ratio of each tissue component.

Figure 3a–d. The area ratios of collagen, elastic fibers, nucleus, and cytoplasm were 6.2%, 2.2%, 10.6%, and 81.0%, respectively, for mild fibrosis. The area ratios for severe fibrosis were 16.7%, 4.6%, 8.5%, and 70.2%, respectively. The area ratios of collagen as well elastic fibers were higher for patients with severe fibrosis than for those with mild fibrosis.

Median area ratios of collagen and elastic fibers

Previous papers reported that pre-existing fibrous tissue, such as muscle and large blood vessels (enclosed by the dotted line in Fig. 4a), should be trimmed from the WSI prior to implementing image analysis.[8,9] The measurements show that without trimming the pre-existing fibrous tissue,

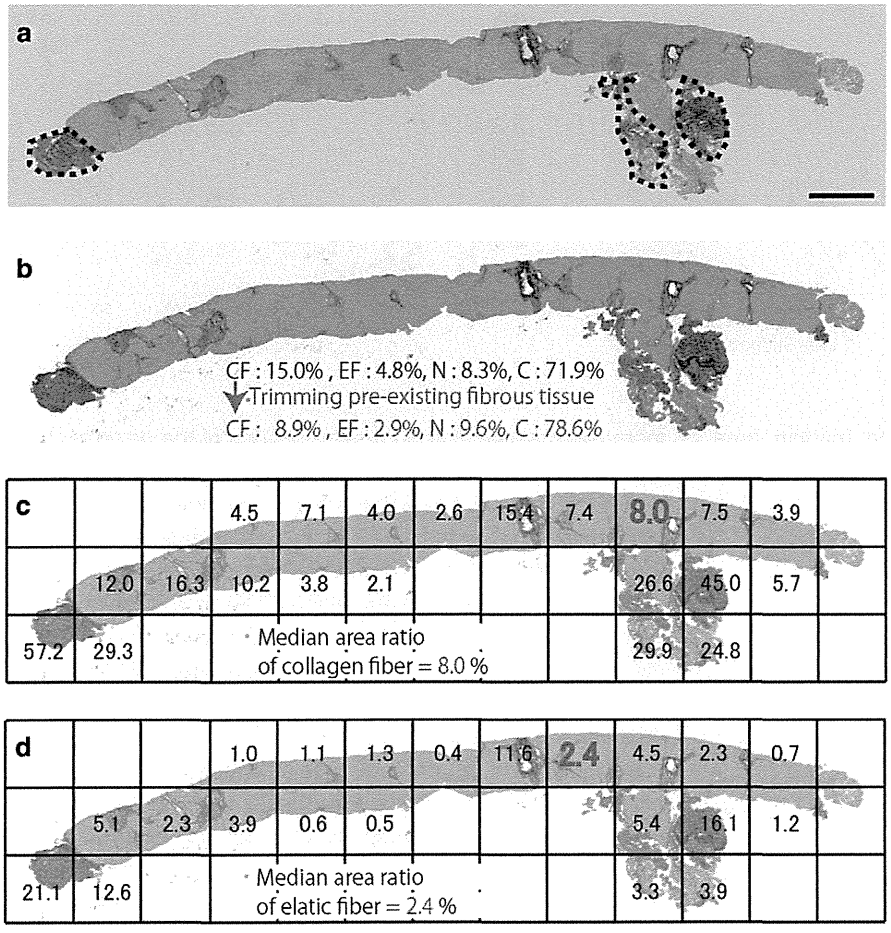

Figure 4 Median area ratios of collagen and elastic fibers. (**a,b**) Whole-slide image (WSI) and classification result of the liver biopsy specimen with mild fibrosis. (**c,d**) Median area ratios of collagen and elastic fibers, respectively, when the classification result was divided into 1×1 mm^2. Black numbers indicate area ratios of each fiber for any tiles where the tissue area occupied at least 20% of the tile area. The red number was the median area ratio of each fiber. Scale bar, 1 mm.

Table 1 Correlation between the median area ratio and area ratio after trimming the pre-existing fibrous tissue from the whole slide image

Tile size (mm^2)	0.01^2	0.25^2	0.50^2	0.75^2	1.00^2	1.25^2	1.50^2
Spearman's rank correlation coefficient							
Collagen fiber	0.79**	0.94**	0.98**	0.97**	0.98**	0.95**	0.93**
Elastic fiber	0.59**	0.87**	0.93**	0.93**	0.95**	0.92**	0.88**

**$P < 0.01$.

the area ratios of collagen and elastic fibers were 15.0% and 4.8%, respectively. After trimming, the area ratios of collagen and elastic fibers were 8.9% and 2.9%, respectively (Fig. 4b).

We then calculated the median area ratios of collagen and elastic fibers from the image tiles of WSI (Fig. 4c,d). The WSI was divided into small tiles of 1×1 mm^2. Then area ratios of each fiber on any tile, where the tissue area occupied at least 20% of the tile area, was calculated. The median area ratios of collagen and elastic fibers were determined as 8.0% (Fig. 4c) and 2.4% (Fig. 4d), respectively.

In order to determine the appropriate tile size, correlation between the median area ratios in other tile sizes and the area ratio after trimming were evaluated for all 38 liver biopsy specimens (Table 1). When the tile size was 1×1 mm^2, the median area ratios of the fibers correlated with the area ratio after trimming most strongly.

Relationship between the area ratio of fiber and liver stiffness

Correlation between the median area ratio of each fiber and liver stiffness measured by transient elastography was evaluated (Fig. 5a,b). Liver stiffness correlated well with the median area ratios of both types of fibers using a tile size of 1×1 mm^2 (collagen fiber: $r = 0.73$ [$P < 0.01$]; elastic fiber: $r = 0.53$ [$P < 0.01$]), as well as the area ratios after trimming pre-existing fibrous tissue off from WSI (collagen fiber: $r = 0.73$ [$P < 0.01$], elastic fiber: $r = 0.51$ [$P < 0.01$]). Liver

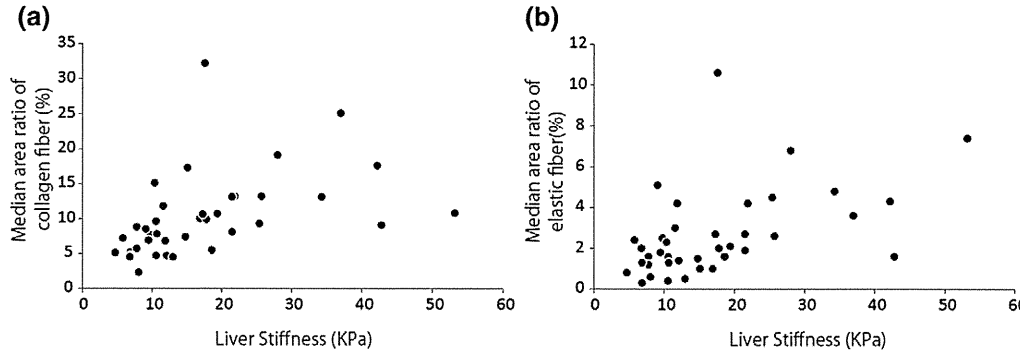

Figure 5 Scatter plot of liver stiffness by transient elastography versus median area ratios of (**a**) collagen and (**b**) elastic fibers. The tile size was 1×1 mm^2 when calculating the median area ratios of both fibers.

stiffness showed better correlation with the median area ratios of both fibers than with the area ratios including pre-existing fibrous tissue (collagen fiber: $r = 0.62$ [$P < 0.01$], elastic fiber: $r = 0.44$ [$P < 0.01$]).

DISCUSSION

Our color classification technique successfully labeled the WSI pixels of EVG-stained liver biopsy specimens in the appropriate classes (collagen, elastic fibers, nucleus, cytoplasm, and glass slide). Even fine collagen and elastic fibers, associated with chronic hepatitis, were accurately detected. Our results suggest that the precise recognition of tissue components in WSIs could identify not only portal fibrosis in patients with chronic viral hepatitis, but also fine pericellular fibrosis in those with alcoholic and non-alcoholic fatty liver diseases.

Pre-existing fibrous tissue such as skin, muscle and large blood vessel affects the accuracy of liver fibrosis measurements.[8] Previous studies have reported that the area ratio of collagen fiber was calculated after trimming pre-existing fibrous tissue from WSI.[8,9] Our study indicates that the trimming step could be avoided by calculating the median area ratios of collagen and elastic fibers from the image tiles of WSI. This approach can minimize the human factor and serve to establish an objective and automated quantification method. This type of image processing is one of the advantages of WSI analysis. We believe that more beneficial and useful algorithms will be developed in the near future.

Liver stiffness measured by transient elastography has been reported to correlate with the liver fibrosis stages.[7] Our results show that liver stiffness had a better correlation with the median area ratios of fibers than with the area ratios of fibers, including pre-existing fibrous tissue. This result suggests that the median area ratio of each fiber increases the correlation with liver stiffness and reflects the progression of liver fibrosis quantitatively. The liver stiffness, especially, correlated better with the median area ratio of collagen fiber than with the median area ratio of elastic fiber, probably due to an increase in elastic fiber in the late stages of the disease.[19–21] It is also possible that liver stiffness may relate to the width or density of fibrous septa.[30] However, we need to integrate other algorithms or densitometric method in order to measure those parameters and illuminate their relationships. The quantification of collagen and elastic fibers in a large number of cases would contribute to the understanding of the mechanism of fibrosis progression associated with chronic liver disease with different etiology, and would help to evaluate clinical usefulness.

In conclusion, a method for simultaneously quantifying collagen and elastic fibers was developed using WSIs of EVG-stained liver biopsy specimens. Median area ratios of collagen and elastic fibers obtained from the image tiles of WSIs were found to be correlated with liver stiffness measured by transient elastography. This enabled more accurate quantification of liver fibrosis than the area ratio of each fiber, including pre-existing fibrous tissue. Our approach of quantifying liver fibrosis will serve as a useful tool to effectively evaluate liver diseases in routine practice.

ACKNOWLEDGMENTS

This study was supported by the New Energy and Industrial Technology Development Organization (NEDO). The authors thank K. Effendi, M. Iwata, M. Takeichi, Y. Nagafuji, and Y. Hashimoto for technical assistance.

REFERENCES

1 The French METAVIR Cooperative Study Group. Intraobserver and interobserver variations in liver biopsy interpretation in patients with chronic hepatitis C. *Hepatology* 1994; **20**: 15–20.
2 Desmet VJ, Knodell RG, Ishak KG *et al.* Formulation and application of a numerical scoring system for assessing histological activity in asymptomatic chronic active hepatitis [Hepatology 1981; 1: 431–435]. *J Hepatol* 2003; **38**: 382–6.
3 Koda M, Matunaga Y, Kawakami M, Kishimoto Y, Suou T, Murawaki Y. FibroIndex, a practical index for predicting significant fibrosis in patients with chronic hepatitis C. *Hepatology* 2007; **45**: 297–306.

4 Forns X, Ampurdanes S, Llovet JM *et al.* Identification of chronic hepatitis C patients without hepatic fibrosis by a simple predictive model. *Hepatology* 2002; **36**: 986–92.
5 Wai CT, Greenson JK, Fontana RJ *et al.* A simple noninvasive index can predict both significant fibrosis and cirrhosis in patients with chronic hepatitis C. *Hepatology* 2003; **38**: 518–26.
6 Ngo Y, Munteanu M, Messous D *et al.* A prospective analysis of the prognostic value of biomarkers (FibroTest) in patients with chronic hepatitis C. *Clin Chem* 2006; **52**: 1887–96.
7 Ebinuma H, Saito H, Komuta M *et al.* Evaluation of liver fibrosis by transient elastography using acoustic radiation force impulse: Comparison with Fibroscan ®. *J Gastroenterol* 2011; **46**: 1238–48.
8 Standish RA, Cholongitas E, Dhillon A, Burroughs AK, Dhillon AP. An appraisal of the histopathological assessment of liver fibrosis. *Gut* 2006; **55**: 569–78.
9 Calvaruso V, Burroughs AK, Standish R *et al.* Computer-assisted image analysis of liver collagen: Relationship to Ishak scoring and hepatic venous pressure gradient. *Hepatology* 2009; **49**: 1236–44.
10 Goodman ZD, Becker RL Jr, Pockros PJ, Afdhal NH. Progression of fibrosis in advanced chronic hepatitis C: Evaluation by morphometric image analysis. *Hepatology* 2007; **45**: 886–94.
11 Goodman ZD, Stoddard AM, Bonkovsky HL *et al.* HALT-C Trial Group. Fibrosis progression in chronic hepatitis C: Morphometric image analysis in the HALT-C trial. *Hepatology* 2009; **50**: 1738–49.
12 Lazzarini AL, Levine RA, Ploutz-Snyder RJ, Sanderson SO. Advances in digital quantification technique enhance discrimination between mild and advanced liver fibrosis in chronic hepatitis C. *Liver Int* 2005; **25**: 1142–9.
13 McHutchison J, Goodman Z, Patel K *et al.*; Farglitizar Study Investigators. Farglitazar lacks antifibrotic activity in patients with chronic hepatitis C infection. *Gastroenterology* 2010; **138**: 1365–73. 1673 e1–2.
14 O'Brien MJ, Keating NM, Elderiny S *et al.* An assessment of digital image analysis to measure fibrosis in liver biopsy specimens of patients with chronic hepatitis C. *Am J Clin Pathol* 2000; **114**: 712–18.
15 Wright M, Thursz M, Pullen R, Thomas H, Goldin R. Quantitative versus morphological assessment of liver fibrosis: Semi-quantitative scores are more robust than digital image fibrosis area estimation. *Liver Int* 2003; **23**: 28–34.
16 Masseroli M, Caballero T, O'Valle F, Del Moral RM, Perez-Milena A, Del Moral RG. Automatic quantification of liver fibrosis: Design and validation of a new image analysis method: Comparison with semi-quantitative indexes of fibrosis. *J Hepatol* 2000; **32**: 453–64.
17 Hui AY, Liew CT, Go MY *et al.* Quantitative assessment of fibrosis in liver biopsies from patients with chronic hepatitis B. *Liver Int* 2004; **24**: 611–18.
18 Shikata T, Skai T. Elastogenesis in the liver. *Acta Pathol Jpn* 1974; **24**: 21–31.
19 Scheuer PJ, Maggi G. Hepatic fibrosis and collapse: Histological distinction by orecin staining. *Histopathology* 1980; **4**: 487–90.
20 Thung SN, Gerber MA. The formation of elastic fibers in livers with massive hepatic necrosis. *Arch Pathol Lab Med* 1982; **106**: 468–9.
21 Bedossa P, Lemaigre G, Paraf F, Martin E. Deposition and remodelling of elastic fibres in chronic hepatitis. *Virchows Arch A Pathol Anat Histopathol* 1990; **417**: 159–62.
22 Gilbertson JR, Ho J, Anthony L, Jukic DM, Yagi Y, Parwani AV. Primary histologic diagnosis using automated whole slide imaging: A validation study. *BMC Clin Pathol* 2006; **6**: 4.
23 Glatz-Krieger K, Glatz D, Mihatsch MJ. Virtual slides: High-quality demand, physical limitations, and affordability. *Hum Pathol* 2003; **34**: 968–74.
24 Weinstein RS, Graham AR, Richter LC *et al.* Overview of telepathology, virtual microscopy, and whole slide imaging: Prospects for the future. *Hum Pathol* 2009; **40**: 1057–69.
25 Diamond J, Anderson NH, Bartels PH, Montironi R, Hamilton PW. The use of morphological characteristics and texture analysis in the identification of tissue composition in prostatic neoplasia. *Hum Pathol* 2004; **35**: 1121–31.
26 Hashiguchi A, Hashimoto Y, Suzuki H, Sakamoto M. Using immunofluorescent digital slide technology to quantify protein expression in archival paraffin-embedded tissue sections. *Pathol Int* 2010; **60**: 720–25.
27 Puppa G, Risio M, Sheahan K *et al.* Standardization of whole slide image morphologic assessment with definition of a new application: Digital slide dynamic morphometry. *J Pathol Inform* 2011; **2**: 48.
28 Sertel O, Kong J, Shimada H, Catalyurek UV, Saltz JH, Gurcan MN. Computer-aided prognosis of neuroblastoma on whole-slide images: Classification of stromal development. *Pattern Recognit* 2009; **42**: 1093–103.
29 Gonzalez RC, Woods RE. Object recognition. In: Gonzalez RC, Woods RE, eds. *Digital Image Processing*, 3rd edn. Upper Saddle River, NJ: Pearson Prentice Hall, 2010; 896–9.
30 Zhang YG, Wang BE, Wang TL, Ou XJ. Assessment of hepatic fibrosis by transient elastography in patients with chronic hepatitis B. *Pathol Int* 2010; **60**: 284–90.

SUPPORTING INFORMATION

Additional Supporting Information may be found in the online version of this article at the publisher's web-site:

Figure S1 Whole slide images (WSIs) of liver biopsies from 38 chronic viral hepatitis patients.

Figure S2 Color classification results for WSIs.

J Gastroenterol (2013) 48:526–534
DOI 10.1007/s00535-012-0656-2

ORIGINAL ARTICLE—LIVER, PANCREAS, AND BILIARY TRACT

Accumulation of platelets in the liver may be an important contributory factor to thrombocytopenia and liver fibrosis in chronic hepatitis C

Reiichiro Kondo · Hirohisa Yano · Osamu Nakashima · Ken Tanikawa · Yoriko Nomura · Masayoshi Kage

Received: 3 April 2012 / Accepted: 25 July 2012 / Published online: 22 August 2012

Abstract
Background Thrombocytopenia is a marked feature of chronic liver disease and cirrhosis. We tried to clarify whether an accumulation of platelets in the liver contributes to thrombocytopenia and liver fibrosis in chronic liver disease.
Methods Thirty-eight patients who underwent hepatectomy for hepatocellular carcinoma (HCC) with hepatitis C virus infection were included. The locations of platelets and Kupffer cells and the expression of platelet-derived growth factor (PDGF) receptor-β and smooth muscle actin (SMA) were identified by immunohistochemistry. Perisinusoidal mesenchymal cells that express PDGF receptor-β and SMA were interpreted as transformed hepatic stellate cells (HSCs).
Results Patients with cirrhosis had a more extensive platelet area in the liver compared to controls (5601 $\pm$ 5611 vs. 564 $\pm$ 361 μm^2, $p = 0.02$), although the blood platelet count significantly decreased along with the progression of liver fibrosis. In cirrhotic liver, most platelets were present in the sinusoidal space of the periportal area with inflammation, where HSCs expressing PDGF receptor-β were frequently observed. In addition, the platelet and Kupffer cell areas were significantly smaller in cancerous tissue than those in noncancerous tissues (platelet area: 492 $\pm$ 823 vs. 3643 $\pm$ 4055 μm^2, $p = 0.001$; Kupffer cell area: 450 $\pm$ 841 vs. 3012 $\pm$ 3051 μm^2, $p = 0.001$).
Conclusions The accumulation of platelets in the liver with chronic hepatitis may be involved in thrombocytopenia and liver fibrosis through the activation of HSCs. In addition, our findings also indicate that both platelets and Kupffer cells decrease in HCC tissues.

Keywords Platelet · PDGFR-β · Hepatic stellate cells · Sinusoidal endothelial cells

R. Kondo (✉) · H. Yano · K. Tanikawa · Y. Nomura
Department of Pathology, Kurume University School of Medicine, 67 Asahi-machi, Kurume, Fukuoka 830-0011, Japan
e-mail: kondou_reiichirou@kurume-u.ac.jp

R. Kondo · Y. Nomura · M. Kage
Department of Diagnostic Pathology, Kurume University Hospital, 67 Asahi-machi, Kurume, Fukuoka, Japan

O. Nakashima
Department of Clinical Laboratory Medicine, Kurume University Hospital, 67 Asahi-machi, Kurume, Fukuoka, Japan

M. Kage
Research Center for Innovative Cancer Therapy, Kurume University School of Medicine, 67 Asahi-machi, Kurume, Fukuoka, Japan

Introduction

Blood platelets, besides hemostatic properties, have the features of inflammatory cells. Blood platelets, while activated in inflammatory processes, release active compounds: platelet-derived growth factors (PDGF), vascular endothelial growth factor (VEGF), transforming growth factor (TGF)-β, and so forth [1]. Platelets transport these active compounds to the target cells [2, 3]. There are many reports presenting multipotential properties of blood platelets, such as angiogenesis [4–6], wound healing [7, 8], liver regeneration [9], and metastasis in cancer [6, 10, 11]. In acute viral hepatitis, platelets mediate cytotoxic T lymphocyte-induced liver damage [12]. After virus infection, platelets were recruited to the liver, delaying virus elimination and increasing immunopathological liver cell damage [13].

In chronic hepatitis, the blood platelet level gradually decreases, which is reflected in liver fibrosis. Blood

platelets and chronic liver disease are also closely related. Thrombocytopenia is a marked feature of chronic liver disease and cirrhosis. Cirrhosis is a major cause of morbidity and mortality in many countries, and results in liver failure, portal hypertension, and increased risk of carcinogenesis [14]. The main causes of liver fibrosis include chronic hepatitis C virus infection, alcohol abuse, and nonalcoholic steatohepatitis [15]. The role of platelets in the pathogenesis of liver damage and the exact mechanisms leading to thrombocytopenia in cirrhosis are not yet clear [16]. The thrombocytopenia that occurs in cirrhosis is most likely due to various processes, including increased splenic platelet breakdown [17–19], splenic pooling [20, 21], and the inability of the bone marrow to increase platelet production adequately [22]. According to previous reports assessing the feasibility of platelet scintigraphy, an accumulation of platelets in the liver was observed in patients presenting with thrombocytopenia [17–20, 23–25]. Based on these findings, thrombocytopenia with chronic hepatitis and cirrhosis may be caused by hypersplenism, as well as by the capture of platelets by the liver. However, the platelet kinetics of patients with chronic liver disease are not well characterized. Therefore, the aim of the study described in the present paper was to clarify the histopathological findings of platelets in human liver tissue and to elucidate the role of platelets in the pathogenesis of chronic liver disease.

Methods

Tissues

We studied 38 patients who underwent hepatectomy for hepatocellular carcinoma (HCC) with hepatitis C viral infection at the Kurume University Hospital; their clinical backgrounds are shown in Table 1. These cases did not receive preoperative anticancer therapies. Both cancerous tissues and adjacent noncancerous liver tissues were obtained by surgical operation.

Five specimens of liver tissues obtained from patients who underwent hepatectomy for hepatic cavernous hemangioma without chronic hepatitis were used as controls.

The study was performed with informed consent obtained from patients for the use of their liver tissues in the investigation, and was approved by the ethical committee at Kurume University (approved ID number: 11200).

Histopathology

Each tissue was fixed with 10 % formalin, embedded in paraffin, cut into 5 μm sections, and then used for histological and immunohistological analyses. The specimens were stained with hematoxylin and eosin and examined under a light microscope. The histological liver damage of these specimens was evaluated for fibrosis and inflammation according to the classification proposed by the International Association for the Study of the Liver [26, 27]. The severity of fibrosis (stage of disease) was classified as none (stage 0), mild (portal fibrosis; stage 1), moderate (periportal fibrosis; stage 2), severe (bridging fibrosis with lobar distortion; stage 3), and cirrhosis (stage 4), and the inflammatory activity (grade of disease activity) was classified as none (grade 0), minimal (grade 1), mild (grade 2), moderate (grade 3), or severe (grade 4). The pathological features of HCC were evaluated according to the World Health Organization classification [28].

Histopathological diagnosis and classification were performed by four pathologists (R.K., H.Y., O.N., and M.K.).

Table 1 Clinical features of the patients studied in this work

Stage	1	2	3	4
No. of subjects	10	10	8	10
Sex (male/female)	8/2	9/1	6/2	5/5
Age (years)[a]	74 ± 5.0	71 ± 6.9	69 ± 9.9	74 ± 4.2
Grade (1/2)	7/3	3/7	1/7	1/9
Platelet count ($\times 10^4$)[a]	15.8 ± 3.4	13.5 ± 2.5	11.8 ± 5.1	10.6 ± 2.5
HCC (well/moderate/poor)	0/10/0	1/8/1	1/7/0	0/10/0

The severity of fibrosis was classified as none: stage 0, portal fibrosis: stage 1, periportal fibrosis: stage 2, bridging fibrosis with lobar distortion: stage 3, and cirrhosis: stage 4. The inflammatory activity was classified as none: grade 0, minimal: grade 1, mild: grade 2, moderate: grade 3, or severe: grade 4

HCC hepatocellular carcinoma, *well* well differentiated HCC, *moderate* moderately differentiated HCC, *poor* poorly differentiated HCC

[a] Mean ± SD

Immunohistochemical analysis

The avidin–biotin peroxidase complex method was used for immunohistochemistry. We used monoclonal antibodies against CD41 (1:500, Beckman Coulter, Brea, CA, USA), CD68 (1:200, DAKO, Glostrup, Denmark), PDGF receptor-β (1:200, Santa Cruz Biotechnology, Santa Cruz, CA, USA) and smooth muscle actin (1:200, DAKO). CD41 (glycoprotein IIb/IIa complex) is a specific marker for platelets, so a CD41-positive reaction was taken to indicate the presence of platelets. CD68, an anti-human macrophage antibody, is expressed not only in residential macrophages such as Kupffer cells, but also in migrating macrophages. Among

the CD68-positive cells, those in the sinusoidal space or blood space of cancerous tissues with spindle or stellate-shaped cytoplasm, and those partly adhering to the sinusoidal endothelial cells, were evaluated as Kupffer cells. Perisinusoidal mesenchymal cells express PDGF receptor-β as transformed hepatic stellate cells (HSCs) [29–31]. These cells were evaluated as activated HSCs.

Measurement of cells

The area of platelets and Kupffer cells in each specimen was measured using the WinROOF software package (version 6.1, Mitani Corporation, Fukui, Japan). In non-cancerous liver tissues, the areas were measured in five randomly selected periportal regions. In cancerous tissues, five visual fields were randomly selected.

Transmission electron microscopy

The liver was cut into small pieces (approximately 1 mm^3), the specimens were fixed in 2.5 % glutaraldehyde in 0.1 M phosphate buffer, pH 7.4, and they were then post-fixed in 1 % O_8O_4 in 0.1 M phosphate buffer. Next, the specimens were dehydrated through a graded series of ethanol, passed through propylene oxide, and embedded in Epok 812. Ultrathin sections mounted on copper grids were stained with uranyl acetate and lead citrate and observed in a Hitachi (Tokyo, Japan) H-7650 transmission electron microscope.

Statistical analysis

The arithmetic means and standard deviations of our data were calculated using the JMP software package (release 9.0, SAS Institute, Cary, NC, USA). All data are expressed as mean $\pm$ SD, and p values of less than 5 % were considered to indicate significance.

Results

Histological findings

Noncancerous liver tissues of all patients with hepatitis C virus infection showed various degrees of fibrosis and chronic inflammation. The severity of fibrosis was mild (stage 1) in ten patients, moderate (stage 2) in ten patients, and severe (stage 3) in eight patients, while ten patients had cirrhosis (stage 4). The inflammatory activity was minimal (grade 1) in 12 patients and mild (grade 2) in 26 patients. In control tissues, there were a few lymphocytes, but only in the portal area, and neither necroinflammatory reactions nor fibrosis were noted (grade 0, stage 0).

Among the cancerous tissues in 38 cases, 35 cases were moderately differentiated HCCs, two cases were well-differentiated HCCs, and one case was poorly differentiated HCC. In terms of the diameters of the HCCs, there were two cases with an HCC diameter of $\leq$1.0 cm, 11 cases with a diameter of 1.1–2.0 cm, 14 cases with 2.1–3.0 cm, and 11 cases with $\geq$3.0 cm. Comparing the histological differentiation of cancerous tissues, the mean tumor size was 2.6 $\pm$ 0.6 cm in the well-differentiated HCCs, 3.0 $\pm$ 1.8 cm in the moderately differentiated HCCs, and 6.3 cm in the poorly differentiated HCCs. Among the 37 nodular-type HCCs, 24 specimens had clear fibrous capsules at the tumor and nontumor boundary, while 13 cases had no fibrous capsules.

Platelets in noncancerous liver tissues

In all noncancerous liver tissues, including patients with chronic hepatitis or cirrhosis and in the controls, there were platelets but no megakaryocytes in the sinusoidal space. Patients with cirrhosis had a more extensive platelet area in the noncancerous liver tissue than in controls (5601 $\pm$ 5611 vs. 564 $\pm$ 361 μm^2, $p = 0.02$, $p < 0.05$, Fig. 1a). In patients with chronic hepatitis or cirrhosis, the platelet area in non-cancerous liver tissues increased along with an increase in histological liver damage ($p = 0.02$, $p < 0.05$), although the blood platelet count significantly decreased (Fig. 1b). In noncancerous liver tissues with chronic hepatitis or cirrhosis, platelets were present predominantly in the sinusoidal space of the periportal area with inflammation. In high-stage cases, platelets were observed along the destroyed limiting plate of the expanded fibrous portal area with inflammation, and in the sinusoidal space of the periportal area (Fig. 2).

Relationship among platelets, HSCs, and Kupffer cells in non-cancerous liver tissues

Immunohistochemical studies of noncancerous liver tissues with cirrhosis revealed that most platelets were present in the periportal area with inflammation, where HSCs expressing PDGF receptor-β were frequently observed (Fig. 3a, b). Most smooth muscle actin stained cells were identical to those expressing PDGF receptor-β (Fig. 3c). In noncancerous liver tissues of controls and cases at the lower stage of chronic hepatitis, only a few HSCs expressing PDGF receptor-β were seen.

In noncancerous liver tissues, including patients with chronic hepatitis or cirrhosis and in controls, CD68-positive Kupffer cells were seen in the sinusoidal spaces of both periportal and lobular areas diffusely.

Platelets and Kupffer cells in cancerous tissues

In all cancerous tissues, a few platelets and Kupffer cells were present in the blood spaces of cancerous tissues.

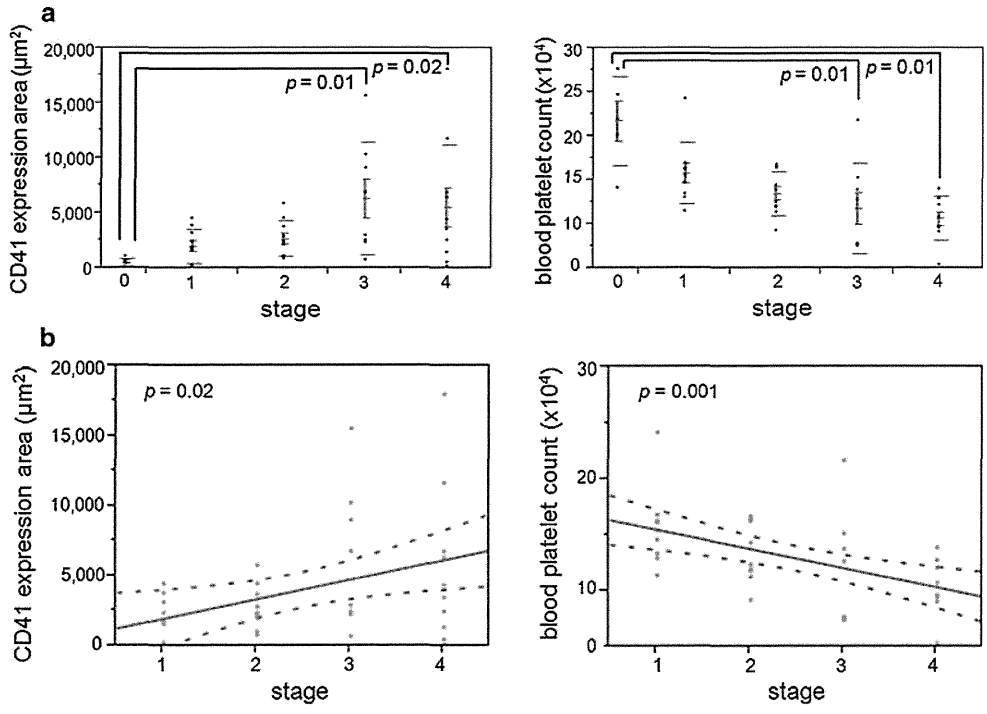

Fig. 1 Relationship between histological liver damage and either the CD41 expression area in the noncancerous liver tissues or the blood platelet count. **a** The noncancerous liver tissues with cirrhosis had a larger CD41 expression area than seen in the controls ($p = 0.02$, $p < 0.05$), although the blood platelet count was small. **b** In the noncancerous liver tissues with chronic hepatitis and cirrhosis, the CD41 expression area increased with increasing histological liver damage ($p = 0.02$, $p < 0.05$), although the blood platelet count decreased ($p = 0.001$, $p < 0.05$)

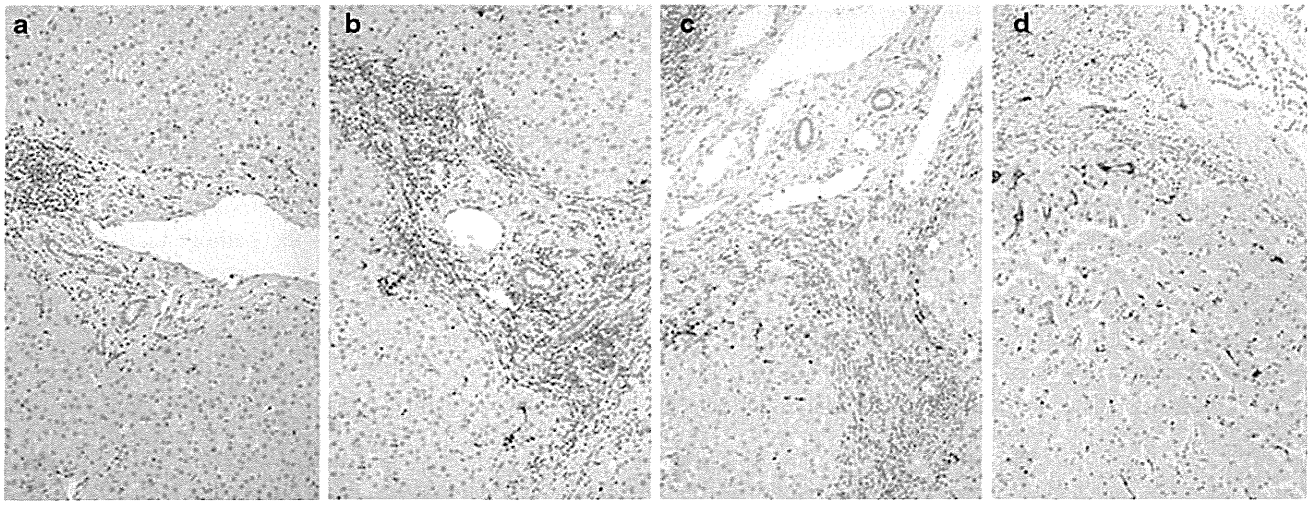

Fig. 2 Typical immunostaining for CD41 in a periportal area of noncancerous liver tissues with chronic hepatitis or cirrhosis. In noncancerous liver tissues with chronic hepatitis or cirrhosis, CD41-positive reactions are present predominantly in the sinusoidal space of the periportal area with inflammation. In high-stage cases, strong CD41 positive reactions are observed along the destroyed limiting plate of the expanded fibrous portal area with inflammation, and in the sinusoidal space of the periportal area. Labeled streptavidin biotin with CD41 antibody: **a** grade 1, stage 1; **b** grade 2, stage 2; **c** grade 2, stage 3; **d** grade 2, stage 4

When the platelet and Kupffer cell areas in the cancerous and non-cancerous tissues were compared, the platelet and Kupffer cell areas were significantly smaller in cancerous tissue than in noncancerous tissue (Fig. 4a, platelet area: 492 ± 823 vs. 3643 ± 4055 μm^2, $p = 0.001$, $p < 0.05$; Fig. 4b, Kupffer cell area: 450 ± 841 vs. 3012 ± 3051 μm^2, $p = 0.001$, $p < 0.05$). Regardless of the liver damage in noncancerous tissue, both the platelet and Kupffer cell areas in cancerous tissue were smaller than those in noncancerous tissue. The platelet and Kupffer cell areas in cancerous tissue tended to decrease with decreasing histological differentiation of HCC (Table 2). We also measured with regard to the

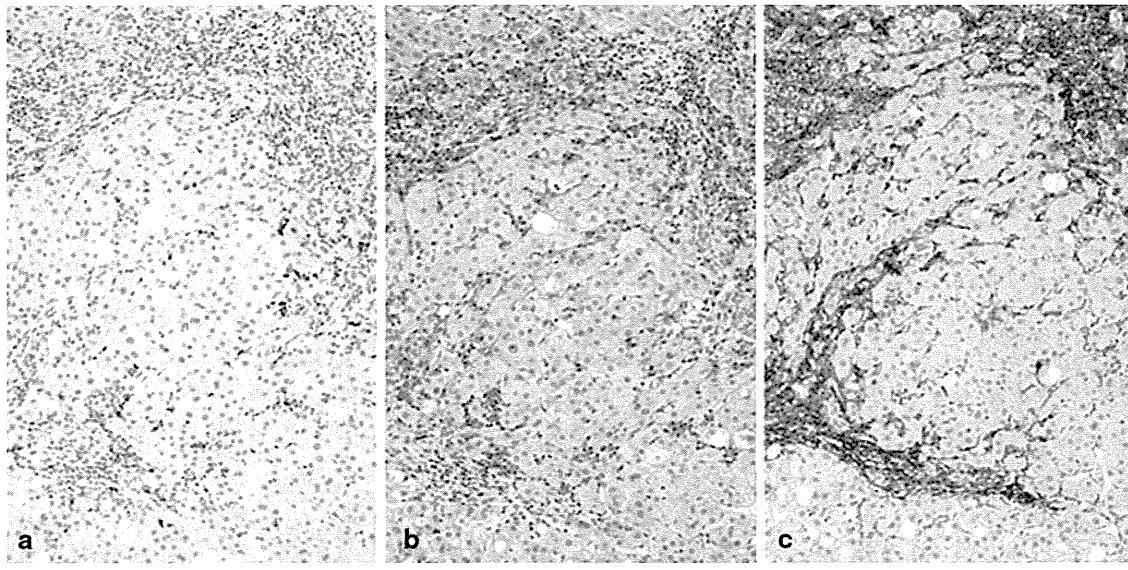

Fig. 3 Typical immunostaining for CD41, PDGF receptor-β, and smooth muscle actin in the periportal area of noncancerous liver tissues with cirrhosis. **a** Platelets are present in the periportal area with inflammation. Labeled streptavidin biotin with CD41 antibody. **b** Serial section shown in **a** stained for PDGF receptor-β antibody. Portal mesenchymal and perisinusoidal cells are stained for PDGF receptor-β. These are dense in the periportal area, where platelets are frequently observed in **a**. Labeled streptavidin biotin with PDGF receptor-β antibody. **c** Serial section shown in **b** stained with smooth muscle actin. Most of the stained cells are identical to those stained for PDGF receptor-β in **b**. Labeled streptavidin biotin with smooth muscle actin antibody

Kupffer cell count. The results evaluated by Kupffer cell count correlate with those evaluated by Kupffer cell areas. The Kupffer cell count was significantly smaller in cancerous tissue than in noncancerous tissue (data was not shown).

Electron microscopic findings

In the sinusoidal space of noncancerous tissues with cirrhosis, there were platelets with dense granules and α-granules. They were partly attached to the sinusoidal endothelial cells (Fig. 5a). Some of the platelets had several empty granules, which are indicative of degranulation (Fig. 5b). Platelets were rarely found in the space of Disse. Around platelets that adhered to the sinusoidal endothelial cells, HSCs that were more spindle-shaped and had a few fat droplets were observed (Fig. 5c). Platelets were not in direct contact with HSCs and Kupffer cells.

Discussion

Blood platelets, by connecting hemostasis and inflammatory processes, participate in the pathogenesis of chronic liver disease. In this study, we demonstrated the pathological findings for the accumulation of platelets in the liver in cases with chronic hepatitis C.

Hill-Zobel et al. [32] studied platelet dynamics in healthy humans using ^{111}In-labeled platelets. They reported

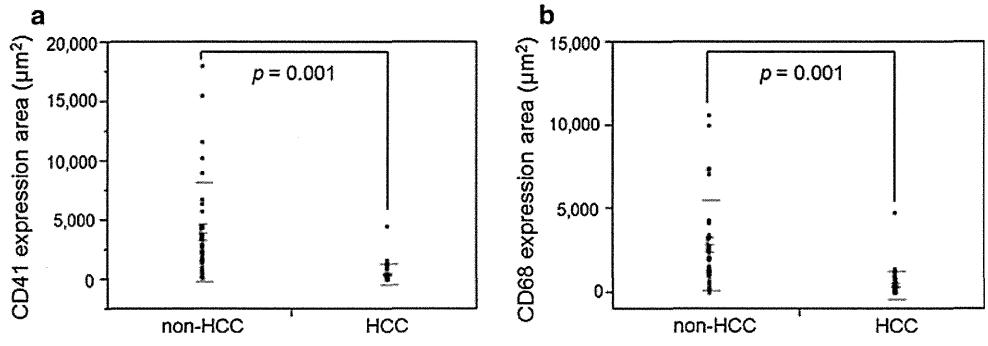

Fig. 4 CD41 (**a**) and CD68 (**b**) expression areas in different tissue types (HCC vs. non-HCC). Both the platelet and Kupffer cell areas are significantly smaller in HCC tissue than those in nonHCC tissue (platelet area: 492 ± 823 vs. 3643 ± 4055 μm^2, $p = 0.001$, $p < 0.05$; Kupffer cell area: 450 ± 841 vs. 3012 ± 3051 μm^2, $p = 0.001$, $p < 0.05$)

that the uptake in the liver was 12.6 % at 30 min and 24 % at ten days, and that in the spleen was 42.7 % at 30 min and 37 % at ten days in healthy humans [32]. The accumulation of platelets in the normal control liver tissue was confirmed in this study. However, the platelet dynamics of patients with chronic hepatitis or cirrhosis are not yet clear. In the current study, we found that the accumulation of platelets in noncancerous liver tissues of patients with chronic hepatitis or cirrhosis increased with increasing histological liver damage. In patients with chronic hepatitis or cirrhosis, the blood platelet level gradually decreased, and was reflected in the liver damage. As there are no megakaryocytes in liver tissues, we can distinguish between platelets that have accumulated in the sinusoidal space and are derived from bone marrow from those derived from extramedullary hematopoiesis. The extramedullary hematopoietic tissue should have hematinic cells, such as megakaryocytes, and immature cells. The accumulation of platelets in the cirrhotic liver with thrombocytopenia has been shown using platelet scintigraphy [17, 23–25]. In patients with thrombocytopenia, Kinuya et al. [24] reported that the spleen/liver uptake ratio for ^{111}In- or ^{99}Tc-labeled platelets was apparently lower in patients for whom splenectomy is ineffective than in those for whom it was effective. Sata et al. [25] reported that platelets were captured in the liver during interferon therapy for chronic hepatitis B, and that this phenomenon is one cause of the decrease in peripheral blood platelets during interferon therapy. The results of our present study are not necessarily contrary to the established theory of thrombocytopenia with chronic hepatitis. It has been reported that the mechanisms leading to thrombocytopenia in cirrhosis most likely involve multifactorial processes [17–22]. We consider that the accumulation of platelets in the liver with chronic hepatitis and cirrhosis may be one of the important contributory factors to thrombocytopenia.

Table 2 Relationship between histological differentiation and platelet area or Kupffer cell area in HCCs

Histological differentiation	Platelet area (μm^2)	Kupffer cell area (μm^2)
Well ($n = 2$)[a]	1532 ± 26	2674 ± 3094
Moderate ($n = 35$)[a]	440 ± 82	305 ± 405
Poor ($n = 1$)	225	108

well well differentiated HCC, *moderate* moderately differentiated HCC, *poor* poorly differentiated HCC

[a] Mean ± SD

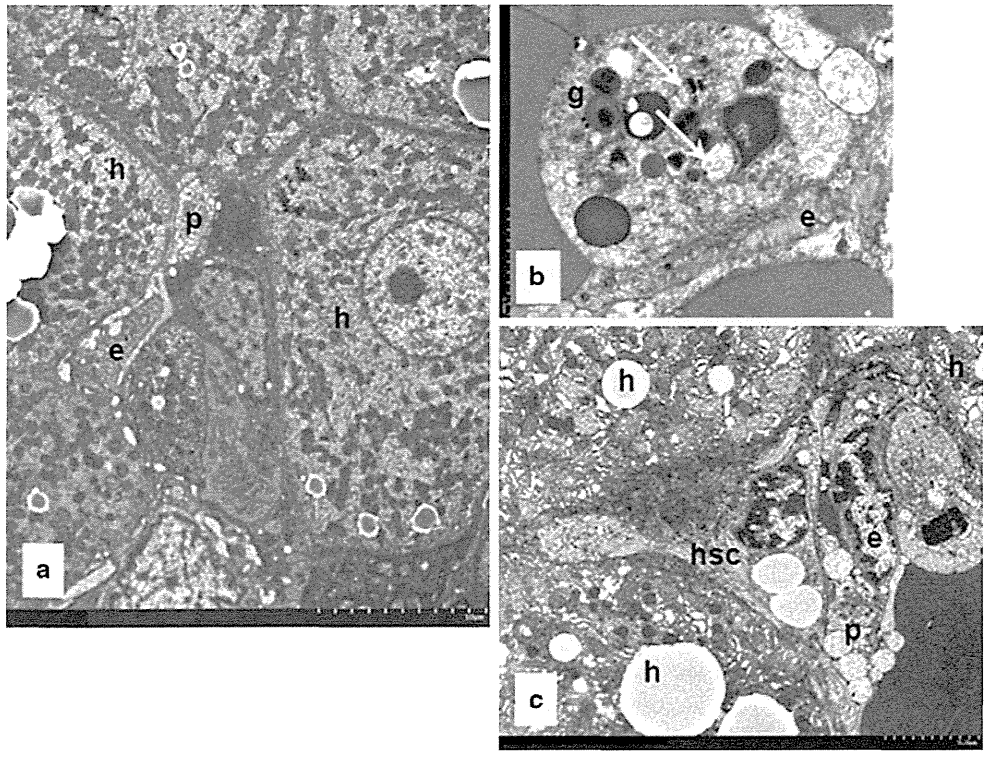

Fig. 5 Electron micrographs of a cirrhotic liver. **a** Platelets (*p*) in the sinusoidal space adhere to endothelial cells (*e*). **b** A platelet that has adhered to a sinusoidal endothelial cell contains both α-granules (*g*) and empty ones (*arrows*). **c** Around platelets that have adhered to a sinusoidal endothelial cell, a hepatic stellate cell (*hsc*)—which is more spindle-shaped, and has a few fat droplets—can be observed. *h* hepatocytes; **a** ×5000, **b** ×25000; **c** ×7000

Histologically, platelets in noncancerous liver tissues of patients with chronic hepatitis or cirrhosis are seen predominantly in the sinusoidal space of the periportal area with inflammation. As viewed through an electron microscope, the platelets aggregate in the sinusoids and adhere to the sinusoidal endothelial cells. Platelets contain four types of distinguishable granules or vesicles: dense granules, lysosomes, peroxisomes, and α-granules. These granules contain various active compounds. Blood platelets, activated in inflammatory and immune processes, release different intraplatelet compounds [1]. Platelets transport these active compounds in their granules to the target cells [2, 3]. Platelets then adhere to endothelial cells or exposed subendothelial matrices. Following adhesion, they become activated and secrete granule content. The accumulation of platelets in the liver and the adhesion to the sinusoidal endothelial cells are important steps in direct platelet action for the liver. In blood vessels, the vessel wall, with its inner lining of endothelium, is crucial to the maintenance of a patent vasculature. The endothelium contains thromboregulators—nitric oxide, prostacyclin, and the ectonucleotidase CD39—which together provide a defence against platelet thrombus formation [33]. When the endothelium is disrupted, collagen and tissue factor become exposed to the flowing blood, thereby initiating the formation of thrombus. Endothelium is also an important target for tumor necrosis factor (TNF) and interleukin-1 (IL-1). The endothelium synthesizes and releases platelet activating factor (PAF) in response to TNF. This activity of TNF overlaps that of IL-1, which also induces PAF production in endothelium [34]. These vessel wall alterations result in a change in endothelium from antithrombotic to thrombotic. The disrupted endothelium is the first reaction in platelet adhesion to the vessel subendothelium under physiologic blood flow [33]. In the presence of TNF-α-induced sinusoidal alteration, platelets adhere to sinusoidal endothelial cells in the same way as to vessel walls [35]. Characteristic pathological features of chronic HCV infection are chronic inflammation and apoptosis of infected and bystander hepatocytes [36, 37]. In a model of hepatitis, Kupffer cells produced the majority of TNF-α [38]. Under lipopolysaccharide administration in mice, TNF or IL-1 induce platelets to accumulate in the liver sinusoidal space within a few minutes by a different mechanism of aggregation [39–41]. With the depletion of Kupffer cells, platelets do not accumulate in the liver after lipopolysaccharide administration [41]. Kupffer cells are involved in various mechanisms, such as phagocytosis, metabolism, cytokine generation, and antitumor effect. Platelets may accumulate in the sinusoidal space under thrombocytotic conditions in chronic hepatitis C brought about by the activated hepatic reticuloendothelial system, as caused by inflammation through the mechanism involving the activation of Kupffer cells.

The role of platelets in the pathogenesis of chronic hepatitis and cirrhosis is not clear. We suggest that platelet-derived factor and liver condition should be taken into account when examining the role of platelets in the liver. We identified a dense population of cells expressing PDGF receptor-β in the periportal areas of cirrhotic liver, whereas only a few mesenchymal cells stained for this peptide were seen in patients at the lower stage of chronic hepatitis and in controls. In addition, most of the PDGF receptor-β expressing cells were also stained for smooth muscle actin. These cells, which play a central role in liver fibrosis, are believed to be transformed from HSCs [29–31], and their proliferation is stimulated by PDGF [42]. HSCs are increasingly being seen as key mediators in the progression of liver fibrosis. In this study, HSCs expressing PDGF receptor-β were located in the periportal area, where platelets were frequently observed. PDGF is the basic mediator involved in platelet granules. PDGF overexpression has been linked to different types of fibrotic disorders and malignancies [43]. In chronic liver disease, the essential role of all PDGF family members in liver fibrosis has been demonstrated [42, 44–47]. To date, four members of the PDGF family have been identified: PDGF-A, PDGF-B, PDGF-C, and PDGF-D [48]. PDGF-B has a stimulating influence on the fibrogenesis and mitogenesis of HSCs in the liver [42]. The biological effects of PDGF are elicited through binding to two specific receptors, PDGF receptor-α and PDGF receptor-β. The binding affinity of PDGF receptor-β is restricted to PDGF-B [49]. When HSCs expressing PDGF receptor-β are present in the liver, the liver may be susceptible to PDGF contained in platelets. The accumulation of platelets in the liver with chronic hepatitis may be involved in liver fibrosis through the activated HSCs.

We also found that the platelet area was significantly smaller in cancerous tissue than that in noncancerous tissues. It has been reported that the number of Kupffer cells in cancerous tissues decreased in comparison with the number in noncancerous tissues as the histological differentiation of HCC decreased [50]. Indeed, the Kupffer cell area in cancerous tissues was significantly smaller than that in noncancerous tissues and tended to decrease with decreasing histological differentiation of HCC in this study. We consider that platelets may also accumulate in the blood space in cancerous tissue through some mechanisms involving the Kupffer cells.

In conclusion, the results obtained in the present study indicate that the accumulation of platelets in the liver with chronic hepatitis C may be involved in thrombocytopenia and liver fibrosis through the activated HSCs. In addition, platelets may accumulate in the sinusoidal space through another mechanism involving the activation of Kupffer cells. Further study of the biological characteristics and

function of these cells will contribute to improving the treatment of thrombocytopenia and liver fibrosis.

Conflict of interest The authors declare that they have no conflict of interest.

References

1. Mannaioni PF, Di Bello MG, Masini E. Platelets and inflammation: role of platelet-derived growth factor, adhesion molecules and histamine. Inflamm Res. 1997;46:4–18.
2. Handagama PJ, George JN, Shuman MA, McEver RP, Bainton DF. Incorporation of a circulating protein into megakaryocyte and platelet granules. Proc Natl Acad Sci USA. 1987;84:861–5.
3. Verheul HMW, Hoekman K, Bakker SL, Eekman CA, Folman CC, Broxterman HJ, et al. Platelet: transporter of vascular endothelial growth factor. Clin Cancer Res. 1997;3:2187–90.
4. Italiano JE Jr, Richardson JL, Patel-Hett S, Battinelli E, Zaslavsky A, Short S, et al. Angiogenesis is regulated by a novel mechanism: pro- and antiangiogenic proteins are organized into separate platelet α granules and differentially released. Blood. 2008;111:1227–33.
5. Brill A, Dashevsky O, Rivo J, Gozal Y, Varon D. Platelet-derived microparticles induce angiogenesis and stimulate post-ischemic revascularization. Cardiovasc Res. 2005;67:30–8.
6. Janowska-Wieczorek A, Wysoczynski M, Kijowski J, Marquez-Curtis L, Machalinski B, Ratajczak J, et al. Microvesicles derived from activated platelets induce metastasis and angiogenesis in lung cancer. Int J Cancer. 2005;113:752–60.
7. Gilsanz F, Escalante F, Auray C, Olbes AG. Treatment of leg ulcers in β-thalassaemia intermedia: use of platelet-derived wound healing factors from the patient's own platelets. Br J Haematol. 2001;115:710.
8. Mazzucco L, Medici D, Serra M, Panizza R, Rivara G, Orecchia S, et al. The use of autologous platelet gel to treat difficult-to-heal wounds: a pilot study. Transfusion. 2004;44:1013–8.
9. Lesurtel M, Graf R, Aleil B, Walther DJ, Tian Y, Jochum W, et al. Platelet-derived serotonin mediates liver regeneration. Science. 2006;312:104–7.
10. Nash GF, Turner LF, Scully MF, Kakkar AK. Platelets and cancer. Lancet Oncol. 2002;3:425–30.
11. Camerer E, Qazi AA, Duong DN, Cornelissen I, Advincula R, Coughlin SR. Platelets, protease-activated receptors, and fibrinogen in hematogenous metastasis. Blood. 2004;104:397–401.
12. Iannacone M, Sitia G, Isogawa M, Marchese P, Castro MG, Lowenstein PR, et al. Platelets mediate cytotoxic T lymphocyte-induced liver damage. Nat Med. 2005;11:1167–9.
13. Lang PA, Contaldo C, Georgiev P, El-Badry AM, Recher M, Kurrer M, et al. Aggravation of viral hepatitis by platelet-derived serotonin. Nat Med. 2008;14:756–61.
14. Bataller R, Brenner DA. Liver fibrosis. J Clin Invest. 2005; 115:209–18.
15. Friedman SL. Liver fibrosis-from bench to bedside. J Hepatol. 2003;38(Suppl 1):S38–53.
16. Witters P, Freson K, Verslype C, Peerlinck K, Hoylaerts M, Nevens F, et al. Review article: blood platelet number and function in chronic liver disease and cirrhosis. Aliment Pharmacol Ther. 2008;27:1017–29.
17. Aoki Y, Hirai K, Tanikawa K. Mechanism of thrombocytopenia in liver cirrhosis: kinetics of indium-111 tropolone labelled platelets. Eur J Nucl Med. 1993;20:123–9.
18. Schmidt KG, Rasmussen JW, Bekker C, Madsen PE. Kinetics and in vivo distribution of 111-In-labelled autologous platelets in chronic hepatic disease: mechanisms of thrombocytopenia. Scand J Haematol. 1985;34:39–46.
19. Toghill PJ, Green S. Splenic influences on the blood in chronic liver disease. Q J Med. 1979;48:613–25.
20. Aster RH. Pooling of platelets in the spleen: role in the pathogenesis of "hypersplenic" thrombocytopenia. J Clin Invest. 1966; 45:645–57.
21. Peck-Radosavljevic M. Thrombocytopenia in liver disease. Can J Gastroenterol. 2000;14:60D–6D.
22. Kajihara M, Okazaki Y, Kato S, Ishii H, Kawakami Y, Ikeda Y, et al. Evaluation of platelet kinetics in patients with liver cirrhosis: similarity to idiopathic thrombocytopenic purpura. J Gastroenterol Hepatol. 2007;22:112–8.
23. Noguchi H, Hirai K, Aoki Y, Sakata K, Tanikawa K. Changes in platelet kinetics after a partial splenic arterial embolization in cirrhotic patients with hypersplenism. Hepatology. 1995;22: 1682–8.
24. Kinuya K, Matano S, Nakashima H, Taki S. Scintigraphic prediction of therapeutic outcomes of splenectomy in patients with thrombocytopenia. Ann Nucl Med. 2003;17:161–4.
25. Sata M, Yano Y, Yoshiyama Y, Ide T, Kumashiro R, Suzuki H, et al. Mechanism of thrombocytopenia induced by interferon therapy for chronic hepatitis B. J Gastroenterol. 1997;32: 206–10.
26. Desmet VJ, Gerber M, Hoofnagle JH, Manns M, Scheuer PJ. Classification of chronic hepatitis: diagnosis, grading and staging. Hepatology. 1994;19:1513–20.
27. Batts KP, Ludwig J. Chronic hepatitis. An update on terminology and reporting. Am J Surg Pathol. 1995;19:1409–17.
28. Hirohashi S, Blum HE, Ishak KG, Deugnier Y, Kojiro M, Laurent Puig P, et al. Tumours of the liver and intrahepatic bile ducts. Hepatocellular carcinoma. In: Hamilton SR, Aaltonen LA, editors. Pathology and genetics of tumor of the digestive system. World Health Organization Classification of Tumors. Lyon: IARC Press; 2000. p. 159–72.
29. Pinzani M, Milani S, Herbst H, DeFranco R, Grappone C, Gentilini A, et al. Expression of platelet-derived growth factor and its receptors in normal human liver and during active hepatic fibrogenesis. Am J Pathol. 1996;148:785–800.
30. Blomhoff R, Wake K. Perisinusoidal stellate cells of the liver: important roles in retinol metabolism and fibrosis. FASEB J. 1991;5:271–7.
31. Ikura Y, Morimoto H, Ogami M, Jomura H, Ikeoka N, Sakurai M. Expression of platelet-derived growth factor and its receptor in livers of patients with chronic liver disease. J Gastroenterol. 1997;32:496–501.
32. Hill-Zobel RL, McCandless B, Kang SA, Chikkappa G, Tsan MF. Organ distribution and fate of human platelets: studies of asplenic and splenomegalic patients. Am J Hematol. 1986;23:231–8.
33. Furie B, Furie BC. Mechanisms of thrombus formation. N Engl J Med. 2008;359:938–49.
34. Bussolino F, Camussi G, Baglioni C. Synthesis and release of platelet-activating factor by human vascular endothelial cells treated with tumor necrosis factor or interleukin 1α. J Biol Chem. 1988;263:11856–61.
35. Miyazawa Y, Tsutsui H, Mizuhara H, Fujiwara H, Kaneda K. Involvement of intrasinusoidal hemostasis in the development of concanavalin A-induced hepatic injury in mice. Hepatology. 1998;27:497–506.
36. Rehermann B, Nascimbeni M. Immunology of hepatitis B virus and hepatitis C virus infection. Nat Rev Immunol. 2005;5: 215–29.
37. Spengler U, Nattermann J. Immunopathogenesis in hepatitis C virus cirrhosis. Clin Sci. 2007;112:141–55.
38. Dolganiuc A, Norkina O, Kodys K, Catalano D, Bakis G, Marshall C, et al. Viral and host factors induce macrophage activation and loss of toll-like receptor tolerance in chronic HCV infection. Gastroenterology. 2007;133:1627–36.